1 **Global evaluation of ELMv1-CNP and the role of the phosphorus cycle in the historical**

2 **terrestrial carbon balance**

4 Xiaojuan Yang[1*], Peter Thornton[1], Daniel Ricciuto[1], Yilong Wang[2,3], Forrest Hoffman[4]

5 [1]Environmental Sciences Division, Oak Ridge National Lab, Oak Ridge, TN 37831, USA

6 [2]Key Laboratory of Land Surface Pattern and Simulation, Institute of Geographic

7 Sciences and Natural Resources Research, Chinese Academy of Sciences, Beijing, China

8 [3]Laboratoire des Sciences du Climat et de l'Environnement, CEA-CNRS-UVSQ- Université

9 Paris Saclay, 91191, Gif-sur-Yvette CEDEX, France

10 [4]Computational Sciences & Engineering Division, Oak Ridge National Lab, Oak Ridge, TN

11 37831, USA

17 *Corresponding Author:*

19 **Phone:** 865-5747615

20 **E-mail:** yangx2@ornl.gov

38 **Abstract**

39 The importance of carbon (C)-nutrient interactions to the prediction of future C uptake has long

40 been recognized. The Energy Exascale Earth System Model (E3SM) land model (ELM) version 1

41 is one of the few land surface models that include both N and P cycling and limitation (ELMv1-

42 CNP). Here we provide a global scale evaluation of ELMv1-CNP using International Land Model

43 Benchmarking (ILAMB) system. We show that ELMv1-CNP produces realistic estimates of

44 present-day carbon pools and fluxes. Compared to simulations with optimal P availability,

45 simulations with ELMv1-CNP produces better performance, particularly for simulated biomass,

46 leaf area index (LAI), and global net C balance. We also show ELMv1-CNP simulated N and P

47 cycling are in good agreement with data-driven estimates. We compared ELMv1-CNP simulated

48 response to CO_2 enrichment with meta-analysis of observations from similar manipulation

49 experiments. We show that ELMv1-CNP is able to capture the field observed responses for

50 photosynthesis, growth, and LAI. We investigated the role of P limitation in the historical

51 balance and show that global C sources and sinks are significantly affected by P limitation, as

52 the historical CO_2 fertilization effect was reduced by 20% and C emission due to land use and

53 land cover change was 11% lower when P limitation was considered. Our simulations suggest

54 that introduction of P cycle dynamics and C-N-P coupling will likely have substantial

55 consequences for projections of future C uptake.

56

57

58

59

60

61

62

63

64

65

66

67 *Copyright statement:*

68

69 *This manuscript has been authored by UT-Battelle, LLC under Contract No. DE-AC05-00OR22725 with the*
70 *US Department of Energy. The United States Government retains and the publisher, by accepting the*
71 *article for publication, acknowledges that the United States Government retains a non-exclusive, paid-*
72 *up, irrevocable, world-wide license to publish or reproduce the published form of this manuscript, or*
73 *allow others to do so, for United States Government purposes. The Department of Energy will provide*
74 *public access to these results of federally sponsored research in accordance with the DOE Public Access*
75 *Plan (http://energy.gov/downloads/doe-public-access-plan).*

76
77

78

79

80

81

82

83

84

85

86

87

88

89

90

91

92

93

94

95

96

97

98

99

1. Introduction

100

101 The recent global carbon (C) budget showed that over the last half century global

102 fossil CO_2 emissions have increased from about 3 Pg C/yr in 1960s to about 9.5 PgC/yr in the

103 last decade (Friedlingstein et al., 2019). It has also been shown that land ecosystems play

104 important roles in controlling the fractions of CO_2 emissions that remain in the atmosphere

105 by taking up about 29% of total emissions (Le Quéré et al., 2018). Large uncertainties

106 remain on the net land-atmosphere C exchange, mainly due to difficulties in quantifying the

107 complex C cycle processes such as CO_2 fertilization effects, responses of carbon fluxes to

108 temperature and precipitation variation, and C emissions associated with land use and land

109 cover change (LULCC). These uncertainties will very likely hamper our ability to predict the

110 future trajectories of atmospheric CO_2.

111 One of the important uncertainties relates to our understanding of C-nutrient

112 interactions and nutrient limitation and how they are represented in models. The

113 importance of nitrogen (N) availability to predicted land C storage has been long recognized

114 (Hungate et al., 2003). Although there were only two models in CMIP5 (the fifth phase of

115 the Coupled Model Intercomparison Project) that accounted for N dynamics and N

116 limitation (Thornton et al., 2007; Thornton et al., 2009; Arora et al., 2013), many ESMs

117 participating in CMIP6 (the Coupled Model Intercomparison Project phase 6) are now

118 including N cycle and C-N interactions (Davies-Barnard et al., 2020; Lawrence et al., 2019;

119 Goll et al., 2017a; Smith et al., 2014; Sellar et al., 2019). The comparisons between these

120 models have been summarized in Arora et al. (2020) and Davies-Barnard et al. (2020). In

121 recent years, significant efforts have also gone into understanding phosphorus (P) cycle

122 dynamics and the role of P limitation in land C storage (Jiang et al., 2019; Hou et al., 2020;

123 Reed et al., 2015; Wieder et al., 2015b; Sun et al., 2017). Increasing numbers of models

124 have developed the capability to include P cycle processes and C-N-P interactions (Wang et

125 al., 2010; Goll et al., 2012; Thum et al., 2019; Goll et al., 2017b; Yang et al., 2014; Yang et al.,

126 2019; Sun et al., 2021). It has been shown that considering P cycle dynamics and C-N-P

127 interactions improves process representation and model fidelity compared with

128 observational and experimental data in most models (Goll et al., 2017b; Yang et al., 2014).

129   Model simulations have also demonstrated the importance of P limitation to land C uptake

130   (Zhang et al., 2014; Goll et al., 2012; Yang et al., 2016; Yang et al., 2019; Sun et al., 2021).

131   Using an ensemble of 14 terrestrial ecosystem models to simulate the planned free-air CO_2

132   enrichment experiment AmazonFACE, Fleischer et al. (2019) showed that P availability

133   reduced the projected CO_2-induced C sink by about 50% compared to estimates from

134   models assuming no phosphorus limitation. Taken together, understanding and

135   representation of the role of P cycle dynamics in affecting terrestrial C balance is essential

136   for the prediction of future terrestrial carbon uptake and atmospheric CO_2 concentration.

137   Despite these recent efforts, P cycle dynamics and C-N-P interactions are not yet

138   included in most CMIP6 models. The Energy Exascale Earth System Model(E3SM) is one of

139   the few models that have been developed a coupled C-N-P capability in the land component

140   in CMIP6 (Burrows et al., 2020). The land model in E3SM, herein referred to as ELMv1-CNP,

141   has been first applied in the Amazon region to test its capability and to evaluate the

142   importance of P limitation in this region (Yang et al., 2019). Yang et al. (2019) provides an in-

143   depth evaluation of ELMv1-CNP for the Amazon rainforest using field observational data,

144   with a focus on how the introduction of P cycle dynamics and P limitation improved model

145   simulated spatial variation of productivity. They show that effects of P limitation on C

146   sources and sinks in the Amazon region are significant, reducing simulated CO_2 fertilization

147   of new carbon uptake by as much as 31%.

148   This study expands the analysis in the Amazon region to the global scale and has two

149   main aims: (1) to provide an evaluation of ELMv1-CNP performance on the global scale

150   using both observational and experimental data, and (2) to quantify the role of P cycle

151   dynamics and P limitation in affecting simulated C sources and sinks globally. We first

152   evaluate the performance of ELMv1-CNP using the ILAMB benchmarking system (Collier et

153   al., 2018), which has been widely used in the evaluation of land surface models and ESMs

154   (Lawrence et al., 2019; Bonan et al., 2019; Zhu et al., 2019; Friedlingstein et al., 2019). We

155   then evaluate ELMv1-CNP simulated N and P pools and fluxes with an observation-based

156   dataset. Realizing that the static benchmarking may not help constrain future model

157   projections, we further evaluate ELMv1-CNP using experimental manipulations of

158   atmospheric CO_2. Finally, we take advantage of the P-enabled capability in ELMv1-CNP to

159   quantify the effect of P dynamics on the simulated ecosystem responses to increasing

160   atmospheric CO_2, increasing N deposition, LULCC, and climate change on the global scale.

161

162   **2. Method**

163   **2.1 Model Overview**

164   ELMv1-CNP is based on the Community Land Model version 4.5 (CLM4.5), which

165   includes coupled C-N biogeochemistry from CLM4 (Thornton et al., 2007) and

166   improvements to canopy photosynthesis, soil biogeochemistry and representation of

167   nitrogen cycle dynamics (Koven et al., 2013; Bonan et al., 2011; Oleson et al., 2013).

168   Recognizing the critical role of the tropical forests in the global carbon cycle and C-climate

169   interactions and the important role of P cycle dynamics and P limitation in tropical forests,

170   we implemented a fully prognostic P cycle and C-N-P interactions into ELMv1-CNP, enabling

171   ELMv1-CNP to be one of the few land surface models that include both N and P cycle

172   dynamics and limitation. The main model features include (1) a fully prognostic P cycle

173   tracking various soil inorganic P pools, vegetation P pools, litter and soil organic P pools (2)

174   the representation of P limitation on plant productivity and litter and soil organic matter

175   decomposition based on a supply-demand approach (3) resolving N vs P limitation using

176   the Liebig law (4) the vertically-resolved soil inorganic and organic P dynamics (5) the

177   decoupling of P cycle from C and N cycle during decomposition due to phosphatase activity

178   (6) the representation of adsorption-desorption dynamics based on soil order.

179   Besides the P cycling processes, the other important difference of ELMv1-CNP from

180   CLM4.5 is the removal of instantaneous downregulation of photosynthesis from nutrient

181   limitation. Instead, longer-term downregulation of productivity is enabled through the

182   implementation of C, N, and P nonstructural vegetation storage pools. In CLM4.5, nutrient

183   limitation is calculated at each time step as a function of potential GPP, stoichiometry of

184   plant tissues, and nitrogen uptake. Any "excess" carbon due to nitrogen limitation is

185   immediately released to the atmosphere through instantaneous downregulation. This

186   nutrient limitation can be highly variable over time and affects diurnal and seasonal cycles

187   of gross primary productivity, which is not consistent with flux tower observations (Ghimire

188   et al., 2016) or with short-term elevated CO_2 experiments that were done with and without

189   nutrient fertilization (Metcalfe et al., 2017). In the current model, competition for available

190   nutrients and plant uptake still occur every timestep given instantaneous demand that is a

191   function of plant GPP and microbial nutrient immobilization (Oleson et al.,

192   2013). However, nutrients taken up by plants are now first allocated to non-structural N

193   and P storage pools instead of directly to structural pools. Nutrient limitation to allocation

194   is determined by comparing plant nutrient demand (given GPP and stoichiometry) and the

195   nutrient availability from the non-structural nutrient pools, which is a function of the pool

196   size in relation to long-term demand. The "excess" carbon flux, which cannot be allocated

197   due to nutrient limitation, is directed to the non-structural plant carbon (NSC) pool instead

198   of downregulating GPP. This pool respires to the atmosphere with a given turnover time.

199   Details about the representation of NSC can be found in the supporting information (Text

200   S1)

201   The model version used in this study is the publicly released ELM v1 and can be

202   downloaded along with all the parameter files at https://github.com/E3SM-Project/E3SM.

203   We also provide the key model parameters in Table S1 (PFT specific) and Table S2 (soil

204   order specific).

2.2 Simulations

206   The simulations presented here were first spun up to bring C, N, and P pools to

207   equilibrium by recycling the GSWP3 (Global Soil Wetness Project Phase 3) climate forcing

208   data (http://hydro.iis.u-tokyo.ac.jp/GSWP3/) between 1901-1920, along with constant

209   atmospheric CO_2, N deposition and land cover type at year 1850. Spinup was accomplished

210   through two steps: accelerated decomposition (AD) spinup and regular spinup. We ran the

211   model for 250 years in the AD spinup mode. The purpose of the AD spinup is to accelerate

212   the decomposition process and speed up the spinup process of the carbon and nutrient

213   cycles. The AD spinup procedure was modified from that originally described by Thornton

214   and Rosenbloom (2005), which used spatially invariant acceleration factors to accelerate

215   decomposition in soil organic matter (SOM) pools. Here we updated the AD spinup by

216   including the impacts of temperature and soil moisture on the acceleration factor. This

217   resulted in higher acceleration factors in cool and/or dry climates, which are typically slower

218   to achieve steady state. In addition, vegetation dead stem and coarse root mortality

219   were accelerated by a factor of 10 to achieve steady state biomass more quickly. In the

220   AD spinup, supplemental soil mineral P was applied for the entire simulation such that there

221   was no P limitation on C and N dynamics. During the transition between AD spinup and

222   regular spinup, we initialized the soil inorganic pools using global P maps developed by

223   (Yang et al., 2013). Since the P cycle involves both biological and geochemical processes

224   that occur on geological time scales, the initialization of P pools provides some reasonable

225   estimates of soil P pools without running the model for millions of simulated years. We

226   then ran normal spinup for 600 years with active C, N, and P coupled biogeochemistry until

227   C, N, and P pools reached equilibrium. The criteria for equilibrium are for global total NEE

228   less than 0.1 PgC/yr averaged over 100 years, the threshold recommended for the C4MIP

229   (Jones et al., 2016). We also ran a control simulation between 1850-2010 as a continuation

230   of the normal spinup. We added the time series of labile P, secondary mineral P and

231   occluded P for the control simulation (Fig. S1). There are very little changes in the inorganic

232   P pools during the 161 years control simulation suggesting that these pools can be

233   considered in equilibrium for the time scale of our interest.

234   After the model was spun up, we ran the global historical transient simulations (1850–

235   2010) at 0.5 degree spatial resolution using GSWP3 v2 climate forcing data, along with

236   historical transient atmospheric CO_2 concentration, N deposition, land use and land cover

237   change that are part of the CMIP6 protocols (https://luh.umd.edu/data.shtml). Input data

238   and references are summarized in Table S3. We also ran a suite of single-factor simulations

239   to examine the individual effects of changing environmental factors. In addition to the ELM

240   v1 simulations with a fully active P cycle, we also performed historical transient and single-

241   factor simulations with P limitation switched off (supplementing P availability to fully meet

242   demand at each grid cell and for each timestep). We denoted the default ELM v1

243   simulations that have an active P cycle as the CNP configuration (ELMv1-CNP) and

244   simulations assuming P saturation (e. g. no P limitation on plant productivity or

245   decomposition) as the CN configuration (ELMv1-CN).

246   We also performed one additional simulation where we initiated a global step increase

247   of atmospheric CO_2 concentration, by +200ppm, starting from 2001 and continuing through

248   2010. These simulations are designed to mimic the Free Air CO_2 Enrichment (FACE)

249   experiments (Ainsworth and Long, 2005). To quantify model sensitivities to elevated CO2,

250   we calculated the effect size (treatment divided by control) over the10 years of simulation

251   (2001-2010).   We then evaluated model sensitivities to elevated CO_2 against meta-analysis

252   from FACE experiments (Ainsworth and Long 2005).

253   All of the simulations are summarized in Table 1.

254

255   2.3. ILAMB

256   We used the International Land Model Benchmarking system (Collier et al., 2018; Luo et

257   al., 2012; Hoffman et al., 2017) to assess the model performance. The ILAMB package is a

258   powerful tool for systematic evaluation of land model performance through comparison

259   with observational data for biogeochemistry, hydrology, radiation and energy, and climate

260   forcing. It was designed to use a wide array of observational data to constrain model

261   results, including various land carbon pools and fluxes, inferred CO2 concentration

262   variability, and functional relationships. For each variable, ILAMB scores model performance

263   for period mean, bias, root-mean-square error (RMSE), spatial distribution, interannual

264   coefficient of variation, seasonal cycle, and long-term trend. These scores are aggregated

265   into an overall score representing multiple aspects of model performance for each variable.

266   These aggregated absolute scores are then used to calculate the relative score, which

267   indicates the relative performance of each model with respect to other models used in the

268   same analysis. ILAMB offers a variety of graphical diagnostics and tabular data to assist the

269   user in understanding when, where, and to what degree model results deviate from

270   observational data. The observational datasets used for the evaluation of carbon cycle in

271   ILAMB are listed in Table S4.

272   In order to understand how the implementation of P cycling dynamics affects model

273   performance, we evaluated the performance of both ELMv1-CNP and ELMv1-CN. In order to

274   provide a context in terms of model performance in ILAMB, we provide the ILAMB

275   evaluation of several other land models included in the Land Surface, Snow and Soil

276   moisture Model Intercomparison Project (LS3MIP) as part of CMIP6 (https://www.wcrp-

277   climate.org/wgcm-cmip/wgcm-cmip6). LS3MIP includes a collection of model experiments

278   including both offline land model experiments and coupled experiments (Van Den Hurk et

279   al., 2016). We used the results from the offline land model experiments. Like our

280   simulations, these experiments were performed at 0.5by0.5 spatial resolution and using the

281   GSWP3 forcing data. Other model configurations in LS3MIP are identical to that used in

282   CMIP6 historical simulations, which we used for the simulations in this study.

283

284   2.4. GOLUM-CNP

285   Since there is no nutrient cycle metrics in ILAMB, we also compared major N and P pools

286   and fluxes along with nutrient use efficiencies from ELMv1-CNP with the data-driven

287   estimates of N and P pools and fluxes from the Global Observation-based Land-ecosystems

288   Utilization Model of Carbon, Nitrogen, and Phosphorus (GOLUM-CNP) (Wang et al., 2018).

289   GOLUM-CNP combines data-driven estimates of N and P inputs and outputs and observed

290   stoichiometric ratios with a steady-state diagnostic model, providing global steady-state N

291   and P pools and fluxes for large biomes. Despite large uncertainties and the steady-state

292   assumptions, GOLUM-CNP provides a global data-driven product that can be used to test

293   nutrient cycles in land surface models.

294

295   **3. Results**

296   **3.1 Evaluations of ELM v1 using ILAMB**

297   ILAMB includes many metrics that cover water, energy, and carbon pools and fluxes on

298   both regional and global scales. Fig. 1 shows ILAMB benchmarking scores for ELMv1-CNP

299   and ELMv1-CN, along with several other land models in CMIP6, which are provided to

300   contextualize ILAMB scores for ELMv1-CNP. The relative model performance scores are

301   shown in Fig. 1, indicating which model version performs better with respect to others. The

302   full results produced by the ILAMB package can be found at https://compy-

303   dtn.pnl.gov/yang954/_build/.

304   Fig. 1 shows that the performance of ELMv1-CNP is comparable to other land models in

305   CMIP6. ELMv1-CNP exhibits performance similar to CLM5 (CESM2) in terms of aggregated

306   scores for carbon cycle metrics, while CLM5 shows better performance with respect to

307   overall functional relationships, mainly due to a better score for functional relationship of

308   burned area. The performance of each model varies for different variables. For example,

309   ORCHIDEE land surface model in IPSL-CM6A-LR performs relatively well in inferred

310   atmospheric carbon dioxide, leaf area index and GPP relationships.

311   Fig.1 also shows the comparison between ELM v1-CNP and ELM v1-CN, allowing us to

312   quantify the impacts of including a prognostic P cycle and realistic P availability on model

313   performance. For metrics in Fig. 1 that show the greatest differences between ELMv1-CNP

314   and ELMv1-CN, the CNP version always has a higher score than CN. This is reflected in the

315   relatively higher aggregated scores for carbon cycle variables and functional relationships

316   in ELMv1 -CNP.

317

318   Fig. 2 shows the Global Net Ecosystem Carbon Balance metric in ILAMB for ELM v1-CNP

319   and ELM v1-CN. The observational data sets for this metric are from the Global Carbon

320   Project (Fig. 2a)(Le Quéré et al., 2016) and from the inversion-based estimate (Hoffman et

321   al., 2014), both providing global totals of land carbon accumulation but for different

322   historical time period (1850-2010 for Hoffman et al., 2014 and 1959-2010 for Le Quere et l.,

323   2016). The simulated global C balance by both ELMv1-CNP and ELMv1-CN are in the range

324   of uncertainty of observational estimates, with ELMv1-CNP simulated historical global

325   carbon accumulation being a better match with mean observational estimates, particularly

326   after 1950. ELMv1-CN estimated a net accumulation of land carbon of 22 Pg C over the

327   period 1850-2010, which is much higher than the mean observational estimate of - 8Pg C.

328   ELMv1-CNP estimated land carbon accumulation of 7 Pg C.

329   Fig. 3 shows the spatial distribution of vegetation biomass for the benchmark data and

330   model bias in ILAMB. Overall both ELMv1-CN and ELMv1-CNP tend to overestimate

331   biomass, compared to this specific global product of biomass (GEOCARBON). The high bias

332   in the tropical region is much reduced in ELMv1-CNP simulations (Fig. 3a, 3b and 3c). The

333   better performance of ELMv1-CNP is also reflected in the spatial Taylor diagram for

334   biomass (Fig. 3d).

335   Another important benchmark in ILAMB is the functional relationships between two

336   variables, for example the relationship between GPP and precipitation and the relationship

337   between LAI and precipitation. An accurate simulation of these relationships in addition to

338   individual benchmarks is an indication that the models are representing the underlying

339   processes correctly. ELMv1-CNP produces a better functional relationship compared to

340   ELMv1-CN. For example, for the relationship between LAI and precipitation ELMv1-CN

341   overestimated LAI, particularly in regions with high precipitation, while the ELMv1-CNP

342   configuration shows an improved relationship (Fig. 4). The improvement of the functional

343   relationship is mainly due to the improvement in high precipitation regions, e.g. lowland

344   tropical forest regions. In these regions, inclusion of P dynamics and P limitation reduced

345   simulated bias in GPP and LAI, therefore leading to better match with the observations.

346

347   3.2. Evaluation of N and P cycling in ELMv1-CNP

348   We evaluated simulated nutrient use efficiencies against that from GOLUM-CNP product

349   on the biome level. Here we define nutrient use efficiency as the ratio between annual NPP

350   and annual nutrient uptake (for both N and P), with NUE for nitrogen use efficiency and

351   PUE for phosphorus use efficiency (Finzi et al., 2007). ELMv1-CNP simulated NUE is higher

352   in temperate and boreal forests and lower in grassland, which is consistent with GOLUM-

353   CNP (Fig. 5a). However, ELMv1-CNP predicted higher NUE in tropical lowland forests than

354   GOLUM-CNP. ELMv1-CNP simulated PUE is also generally consistent with GOLUM -CNP

355   (Fig. 5b). However, ELMv1-CNP simulated PUE in tropical forests is much lower than that

356   from GOLUM-CNP.

357   We also evaluated ELMv1-CNP simulated N and P pools and major fluxes on the global

358   scale for the period of 2001-2010 with the observationally derived products in GOLUM-

359   CNP. Fig. S2 shows the comparison of N and P uptake from ELMv1-CNP and GOLUM-CNP at

360   the biome level. ELMv1-CNP simulated plant N and P uptake is in agreement with GOLUM-

361   CNP, with higher uptake fluxes in tropical forests and lower uptake in temperate and boreal

362   forests. ELMv1-CNP simulated N uptake is lower in the tropical forests, compared to

363   GOLUM-CNP (Fig. S2a). Conversely, simulated P uptake is higher than GOLUM-CNP

364   estimates across the tropics (Fig. S2b).

365

366   **3.2 Evaluations using CO2 manipulation experiment**

367   Relative to the control simulation, increasing atmospheric CO_2 concentration by 200ppm

368   increased gross primary productivity by 23% (global mean) over the 10 years of simulation

369   (2001-2010). Nearly all PFTs showed more than a 10% increase in productivity, with more

370   significant increases occurring in tropical regions and middle latitudes (Fig. 6a). The

371   modeled response ratio of NPP is also showing widespread increases, and on the global

372   scale our results showed a 25.8% increase in NPP in response to CO_2 enrichment (Fig. 6b).

373   The simulated increases in GPP and NPP also showed, to a large extent, translated into

374   increases in vegetation carbon (Fig 6c), with a global average response ratio of 18%. The

375   modeled response ratio of LAI is much smaller, a 5% increase globally (Fig 6d). The globally

376   aggregated simulated effect size of CO_2 enrichment from ELMv1-CNP on GPP, NPP, LAI and

377   NSC compare well to the observations from the meta-analysis (Fig. 7), particularly for GPP

378   and LAI. ELMv1-CNP overestimated the responses of NPP. Both observations and

379   simulations show large sensitivity of NSC to CO2 enrichment, with larger variability in the

380   model simulations.

381

382   **3.3. Carbon, nitrogen and phosphorus pools and fluxes**

383   **3.3.1 Carbon budget**

384   Major components of the global land C budget for present day (mean of 2001–2010) in

385   ELMv1-CNP are shown in Fig 8a. These are from historical simulations with transient climate

386   forcing, atmospheric CO2 concentration, land use and land cover change, and N deposition.

387   For the present day, model simulated total ecosystem C is 2588.73 Pg C, with about 22%

388   stored in vegetation (575.45 Pg C), about 5% stored in litter and coarse wood debris (122.5

389   Pg C), and 73% stored in soil organic matter (1890.78 Pg C). Model simulated vegetation C is

390   within the range of inventory-based estimates from IPCC AR5 (450–650 Pg C). Our simulated

391   vegetation C is also comparable to or slightly higher than observational estimates from the

392   literature: 455Pg C (GEOCARBON, (Avitabile et al., 2016; Santoro et al., 2015), 550±100 Pg C

393   (Houghton, 2003), 560±94 Pg C (Defries et al., 1999), and 450 Pg C (Erb et al., 2018). Model

394   simulated total soil C is within the range of estimates from IPCC AR5 (1500-2400 Pg C) and

395   that from Jobbágy and Jackson (2000) (1750±250 PgC). Model simulated total soil C is lower

396   than several other observational estimates from the literature: 2376-2456 (Batjes, 2014),

397   3000 Pg C (Köchy et al., 2015). As for the top 1m soil carbon, model simulated values are

398   within the range of estimate reported by Todd-Brown et al. (2013) (890-1660 Pg C), but

399   lower than the observational based estimate of 1462–1548 Pg C from Batjes (2014) and

400   1325 Pg C from Köchy et al. (2015). Model simulated litter C (22.9 Pg C) is lower than the

401   observational based estimate: 68 Pg C (Matthews, 1997) and 43±3 Pg C (Pan et al., 2011).

402   Model simulated coarse wood debris C stock (99.6 Pg C) is higher than the observational

403   based estimate: 75 Pg C (Matthews, 1997) and 43±3 Pg C (Pan et al., 2011).

404   Model simulated present day GPP(134.15 Pg C/yr) is slightly higher than observational

405   based estimate: 123±8 Pg C/yr (Beer et al., 2010), 119±6 Pg C/yr (Jung et al., 2011) and 123

406   PgC/yr (IPCC AR5), and lower than 150-175 Pg C/yr from Welp et al. (2011) that is derived

407   based on oxygen isotopes of atmospheric CO_2. A recent study based on satellite data

408   suggested a global GPP of 140 Pg C/yr for year 2007 (Joiner et al., 2018). The comparisons

409   between simulated carbon pools and fluxes and available observations are also included in

410   Table 2.

411

412   **3.3.2. Nitrogen budget**

413   The ELMv1-CNP estimated N budget for the present day (2001–2010) is summarized in

414   Fig 8b. Compared to the C cycle, there are fewer observational estimates for N pools and

415   fluxes. Most of the literature values are from other model simulations. Although not

416   appropriate for direct model evaluation, these modeling estimates from the literature

417   provide a broad context for us to evaluate our simulated pools and fluxes.

418   Model simulated vegetation N is 4.36 Pg N, which is comparable to the estimates from

419   some other modeling studies: 3.8 Pg N (Zaehle et al., 2010; Xu and Prentice, 2008), 5.3 Pg N

420   (Xu and Prentice, 2008) and lower than the estimates of 16 Pg N(Lin et al., 2000) and 18 Pg

421   N (Yang et al., 2009). Model simulated total soil organic matter N is 188.79 Pg N, which is

422   reasonable considering the observational based estimate for 1m of 95 Pg N (Post et al.,

423   1985) and 133–140 Pg N (Batjes, 2014). ELMv1-CNP estimated biological nitrogen fixation

424   (BNF) of 89 TgN/yr is within the range of estimates from literature. Vitousek et al. (2013)

425   estimated that global BNF ranges between 40–100 TgN/yr using a mass-balance approach.

426   A meta-analysis by Davies-Barnard and Friedlingstein (2020) suggested that global inputs of

427   BNF in natural ecosystems range between 52 and 130 TgN/yr, with a median global value of

428   88 TgN/yr. For the purpose of comparison, BNF estimates from CLM5 is 96.4 TgN/yr, slightly

429   higher than our estimate. The comparisons between simulated N pools and fluxes and

430   available observations are also included in Table 2.

431

432

433   **3.3.3   Phosphorus budget**

434

435   The ELMv1-CNP estimated P budget for the present day (2001–2010) is summarized in

436   Fig 8c. Very few observational data are available for P on the global scale. The only

437   observation-based global product is the global P maps developed by (Yang et al., 2013).

438   Model simulated vegetation P is 0.36 Pg P, which is comparable to the estimates from other

439   modeling studies ranging from 0.23 to 3 Pg P (Goll et al., 2012; Wang et al., 2010; Jahnke,

440   1992). Model simulated soil organic P is 3.75 Pg P, which is slightly lower than previous

441   studies 5.74 Pg P (Goll et al., 2012), 5-10 Pg P (Smil, 2000), and 8.6 Pg (Yang et al., 2013).

442   Model simulated soil mineral P for the top 40cm and 60cm is 63.24 and 81.32 respectively,

443   which are generally comparable to the estimate of 45 Pg P for top 50cm soil from Yang et al.

444   (2013). The comparisons between simulated P pools and fluxes and available observations

445   are also included in Table 2.

446

3.4. The effects of P limitation on historical carbon cycle

448   ELMv1-CNP calculates the extent of both N and P limitation for plant growth on the

449   global scale (Figs. 9a and 9b). Generally speaking, P is a more limiting nutrient in tropical

450   evergreen forests and savannas in South America and Africa, while N is more limiting in

451   temperate regions (Fig. 9a). The ratio between the P limitation factor and N limitation

452   factor illustrates the degree of N-P colimitation (Fig. 9b). In many parts of the world, both

453   N and P are limiting productivity.

454   Fig. 10 shows the effects of P dynamics on historical land carbon accumulation.

455   The introduction of P dynamics leads to a 19.5% reduction in C storage due to CO_2

456   fertilization between 1850 and 2010. The consideration of P dynamics also leads to a lower

457   estimate of land use emissions (143.89 PgC vs 161.21 PgC) as CNP simulations generally

458   show lower initial vegetation biomass. Increasing N deposition generally leads to a small

459   carbon accumulation between 1850 and 2010 in both CN and CNP simulations. With P

460   limitation, however, the carbon accumulation from N deposition is reduced by about a

461   third. Climate, although responsible for the large seasonal and interannual variability of

462   carbon fluxes, has only minor impacts on historical carbon accumulation on the global

463   scale for both CN and CNP simulations. When changes of all environmental factors are

464   considered, the impact of P dynamics on carbon accumulation is the balance between a

465   smaller CO_2 fertilization effect and lower land use emissions, with the net effect being

466   slightly lower historical carbon accumulation.

467   Fig. 11 shows the simulated spatial patterns of productivity and carbon storage and

468   how they are affected by P dynamics and limitation. P dynamics strongly control land

469   carbon uptake and storage, particularly in tropical regions. Globally NPP is highest in

470   tropical evergreen forests and lower in middle to high latitude regions. Plant growth in

471   tropical regions, however, is generally limited by P availability, particularly in the central

472   and eastern Amazon basin and tropical Africa. The reduced productivity due to P limitation

473   translates into reduced vegetation carbon storage and soil carbon storage, with the

474   exception of tropical savannas, where fire dynamics also play an important role in

475   vegetation and soil carbon storage.

476

477   **4. Discussions**

478   **4.1. ILAMB benchmarking**

479   This study presents a global assessment of the ELMv1-CNP. Yang et al. (2019) evaluated

480   the performance of ELMv1-CNP in the Amazon region using plot-level observations from the

481   RAINFOR network and found that the model captures well the observed productivity and

482   biomass gradient across the Amazon basin. Here we further evaluate the global model

483   performance using the ILAMB benchmarking system – an open source land model

484   evaluation system that is designed to assess model performance at site level, regional, and

485   global scales in an integrated and comprehensive way.

486   We include several other land models in CMIP6 in our ILAMB analysis with the goal of

487   providing a context for the performance of ELMv1-CNP. We found that ELMv1-CNP exhibits

488   similar performance to other models. It is challenging to demonstrate a clear improvement

489   or degradation for complex land surface models in ILAMB. For example, our analysis

490   indicates that ELMv1-CNP performance is comparable to CLM5 in terms of the overall

491   carbon cycle. Both ELMv1-CNP and CLM5 have a common ancestor CLM4.5, but they took

492   very different approaches for further development. CLM5 had significant efforts undertaken

493   in improving the representation of nitrogen cycle, while ELMv1-CNP was more focused on

494   implementing a prognostic phosphorus cycle and C-N-P interactions. Model development

495   activities in both models helped improved model performance through the lens of ILAMB

496   but the sources of improvements are quite different. This highlights the need to include

497   more process-level evaluations in ILAMB for the purpose of evaluating the impact of specific

498   model improvements.

499   Although CLM5 and ELM-CNP perform similarly in terms of ILAMB scores, it is worth

500   noting the unique role of P cycle dynamics in affecting C cycling and the importance of

501   including P cycle limitation in earth system models for better prediction of carbon-climate

502   feedbacks. The important role of soil P availability in affecting plant growth in tropical

503   forests residing on highly weathered soils has long been recognized (Walker and Syers,

504   1976; Vitousek et al., 2010; Butler et al., 2018; Elser et al., 2007). Recent work has also

505   explored how increasing demand for P may attenuate predicted increase in NPP

506   conceptually by comparing potential demand with potential nutrient availably in the 21st

507   Century (Wieder et al., 2015b; Sun et al., 2017). Increasing numbers of land models have

508   incorporated P cycle dynamics and P limitations (Sun et al., 2021; Nakhavali et al., 2021).

509   Although both N and P limitation acts through reducing NPP, it is critical to include P cycling

510   explicitly in models since P cycle dynamics are very different from the N cycling dynamics.

511   The primary input for P is through rock weathering, which make it a very much non-

512   renewable nutrient for the terrestrial ecosystems, whereas N fixation, the primary input for

513   N, is more biologically driven. P cycling involves the transformation of various forms of P

514   through a series of biological, enzymatical and geochemical processes with the turnover

515   time ranging from seconds to millions of years. N cycle dynamics are relatively simpler, with

516   two inorganic forms and mostly biological and enzymatical processes involved. In addition,

517   the interactions between N and P cycling also points to the need to include P cycle explicitly

518   in land models. Increasing numbers of studies have shown that biological N fixation could

519   be constrained by soil P availability (Hungate et al., 2004; Reed et al., 2013; Barron et al.,

520   2008; Edwards et al., 2006; Crews et al., 2000). On the other hand, studies have also shown

521   that increases in N availability can promote phosphatase activity and enhance biochemical

522   mineralization and therefore accelerate P cycling (Mcgill and Cole, 1981; Wang et al., 2007;

523   Houlton et al., 2008; Olander and Vitousek, 2000; Treseder and Vitousek, 2001; Marklein

524   and Houlton, 2012). We will continue refine and improve the representation of the C-N-P

525   interactions in the future development of ELM.

526   Also, ILAMB, despite being a comprehensive benchmarking tool for land surface models,

527   is limited in scope in terms of the benchmarking data included. For example, Quesada et al.

528   (2012) found that the decreasing west-east gradient in productivity is mostly related to total

529   soil P. Yang et al. (2019) show that consideration of soil P availability improved model

530   simulated productivity, enabling the model to capture the productivity gradient from west

531 to east across the Amazon basin. The problem is that this productivity gradient across the

532 Amazon basin is not captured in ILAMB benchmark data so the "failure" of a CN model

533 would not be captured by ILAMB.

534  We show that the model performance generally improved with realistic P availability

535 through the implementation of a prognostic P cycle in ELM. Compared to ELMv1-CN,

536 ELMv1-CNP simulated biomass has lower bias across the tropical regions as P limitation

537 leads to lower productivity and hence lower biomass. ELMv1-CNP produces better ILAMB

538 scores on the functional relationships between GPP, LAI and other forcing variables, mainly

539 due to improved estimate of GPP and LAI in tropical regions. ELMv1-CNP also produces

540 higher ILAMB scores for the integrated benchmarks such as global net ecosystem carbon

541 balance and carbon dioxide concentration. We note that satisfactory performance for these

542 two integrated metrics is most critical to a land model in ESMs as they are most relevant to

543 the coupling between land ecosystems and radiatively-forced climate change.

544

545  Although the ILAMB benchmarking system is very useful for evaluating model

546 performance from different aspects simultaneously, interpretation of ILAMB scores

547 deserves extra caution with known observational bias considered. For example, ILAMB uses

548 LAI estimated from remote sensing observations from the Moderate Resolution Imaging

549 Spectroradiometer (MODIS) as benchmarking data, while studies have suggested that

550 MODIS LAI may be biased low due to reflectance saturation in dense canopies in the

551 tropical forests (Shabanov et al., 2005; Huete et al., 2002; Kobayashi and Dye, 2005).

552 Another example is the observational data for biomass. There are significant differences

553 between the "tropical" and "GlobalCarbon" datasets and the "GeoCarbon" dataset for

554 tropical biomass, but they were given about the same default weight in the ILAMB scoring

555 system. Mitchard et al. (2014) investigated the marked differences between different

556 estimates of Amazon biomass and suggested the regional biases in some remote sensing

557 products might be due to the lack of consideration of ecological variation in tree wood

558 density and allometry. Further investigation of these datasets is needed to ensure the

559 quality of biomass benchmarking data.

560

561   The current version of ILAMB includes analysis of 28 variables using more than 60

562   datasets or data products. None of these variables, however, are directly related to nutrient

563   cycles. As more land surface models are implementing N and P dynamics, it is becoming

564   increasingly important to include metrics for nutrient stocks and fluxes. Davies-Barnard et

565   al. (2020) assessed five nitrogen-enabled land surface models in CMIP6 and called out the

566   need to have better constraints of nitrogen cycle processes. The need is equally urgent, if

567   not more, to synthesize more observations to better constrain the P cycle processes, as less

568   synthesized data are available for P. Encouragingly, recent studies have started to develop

569   observational datasets based estimate of N and P cycling on the global scale for model

570   evaluation, such as the GOLUM-CNP dataset we used in this study. We hope to highlight the

571   need and engage the broader community in developing additional nutrient datasets that

572   can be included in ILAMB.

573   Other metrics that would be useful are the responses from N and P addition

574   experiments. As Yang et al. (2014) showed, fertilization experiments at sites along the

575   Hawaii chronosequence provided a useful evaluation testbed to assess model simulated

576   responses to N and P fertilization effects. FACE experiments are useful for model evaluation

577   as shown here (section 4.2) and in other studies (Wieder et al., 2019; Davies-Barnard et al.,

578   2020). Warming studies that include an explicit focus on nutrient cycle responses will be

579   another good evaluation opportunity (Melillo et al., 2002). An existing challenge is to

580   provide a common protocol to use these types of experiments in the ILAMB benchmarking

581   system.

582

583   4.2 Evaluations using GOLUM-CNP

584

585   On the biome level ELMv1-CNP simulated nutrient use efficiencies are consistent with

586   the observation-based estimates from GOLUM-CNP. This indicates that the representation

587   of N and P cycling and C-N-P coupling is reasonable in ELMv1-CNP. In terms of nutrient

588   uptake, both show the highest N and P uptake in tropical forests, due to the high N and P

589   demand associated with high productivity. ELMv1-CNP predicted lower N uptake in the

590   tropics, compared to GOLUM-CNP. Nutrient uptake in ELMv1-CNP is a function of nutrient

591   availability and nutrient demand, with demand being determined by available carbon for

592   allocation, allocation fractions to different plant tissues and plant tissue stoichiometry. The

593   simulated NPP at the biome level matches well with NPP from GOLUM-CNP (Fig. S3). The

594   differences in nutrient uptake is therefore likely due to the different C:N and C:P

595   stoichiometric ratios for different vegetation tissues used in ELMv1-CNP and GOLUM-CNP.

596   C:N ratios of leaf, wood, and fine root in GOLUM-CNP are all lower than ELMv1-CNP (21,

597   126, and 40 in GOLUM vs 30, 500, and 42 in ELMv1-CNP). This suggests for given amount of

598   carbon allocation, N uptake would be lower in ELMv1-CNP. C:P ratios of leaf, wood, and

599   fine root in GOLUM-CNP also differ quite significantly from those in ELMv1-CNP (410, 5429,

600   and 1250 in GOLUM vs 600, 3000, and 1000 in ELMv1-CNP). The relatively higher P uptake

601   in ELMv1-CNP can be attributed in large part to the difference in dead wood C:P ratios.

602   Differences in allocation factors could also be contributing to the differences in nutrient

603   uptake between ELMv1-CNP and GOLUM-CNP. For example, the mean allocation fraction to

604   fine root is higher in GOLUM-CNP compared to ELM-CNP, while allocation fraction to leaf is

605   lower in GOLUM-CNP, particularly in forest ecosystems (Fig. S4 and S6). GOLUM-CNP also

606   has higher NPP allocation fraction to woody biomass in boreal forests (Fig. S5)

607

608   **4.3. Evaluations using CO₂ manipulation experiments**

609   Our simulated large increase in GPP with CO$_2$ enrichment (23%) is in agreement with

610   field observations that photosynthetic assimilation increased 28% under elevated CO$_2$

611   (Ainsworth and Long, 2005). Our simulated 26% increase in NPP is higher than the 17%

612   increase in observed increase in dry matter production in the FACE experiments (Ainsworth

613   and Long, 2005; Wieder et al., 2019). Our simulated 18% increase in biomass is higher than

614   the estimates from Terrer et al. (2019), which provides a data-driven estimate of global CO$_2$

615   fertilization effect on biomass and show a relative increase in biomass of 12±3% for a 250

616   ppm CO2 increase. A meta-analysis of woody plants responses to elevated CO2 shows a

617   mean effects of 22.3% on biomass (Baig et al., 2015). Among CLM4, CLM4.5 and CLM5,

618   ELMv1-CNP is more comparable to CLM5 with a strong simulated response of GPP, NPP, and

619   vegetation carbon in response to CO_2 enrichment, while CLM4 and CLM4.5 showed very

620   weak CO_2 effects (Wieder et al., 2019).

621   The much stronger sensitivity of photosynthesis to elevated CO_2 in ELMv1-CNP is due to

622   the removal of instantaneous downregulation of photosynthesis as a response to nutrient

623   limitation. The instantaneous downregulation assumption in CLM4 and CLM4.5 has been

624   shown to be inconsistent with experimental results (Metcalfe et al., 2017). Despite large

625   uncertainty, it is encouraging that simulated NSC response to elevated CO_2 is largely

626   consistent with the observational data (Fig. 7). The low sensitivity of LAI in ELMv1-CNP is

627   also consistent with field observations. Our results suggest the assumption we made

628   regarding the fate of photosynthate is reasonable. Yang et al. (2016) showed that enhanced

629   phosphatase enzyme production response to increasing CO_2 could have important impacts

630   on P availability and sustain forest productivity under elevated CO2. In simulating the

631   planned free-air CO_2 enrichment experiment AmazonFACE, ELMv1-CNP simulated

632   phosphatase activity increased about 20% over 15 years (Fleischer et al., 2019). Here we

633   show that introduction of NSC pools further improve the response of vegetation processes

634   to changes in P availability and P limitation.

635

636   Our findings are consistent with field studies that show the strong increase of NSC under

637   eCO2, particularly when nutrient availability is low (*Wong*, 1990; *Körner et al.* (2005).

638   Several studies evaluating CLM4.5 using carbon isotope data also suggested that model

639   performance would be better with the introduction of an NSC pool (Mao et al., 2016;

640   Raczka et al., 2016; Duarte et al., 2017). Further synthesis of field measurements on NSC in

641   CO_2 enrichment experiments are needed to evaluate and constrain the representation of

642   NSC in models.

643   Our simulated strong sensitivity of photosynthesis to CO2 enrichment is consistent

644   with recent studies that show large GPP growth during the twentieth century (Campbell et

645   al., 2017; Haverd et al., 2020; Ehlers et al., 2015). Ellsworth et al (2017) also showed a large

646   increase of photosynthesis in response to elevated CO_2 in a temperate forest FACE

647   experiment.

648   The increased sensitivity of GPP and NPP to CO_2 enrichment in ELMv1-CNP, compared

649   with the predecessors CLM 4 and CLM4.5, will very likely reduce the bias in the atmospheric

650   fraction of human CO_2 emissions in previous coupled simulations as noted by Hoffman et al.

651   (2014). In fact, CO_2 concentration metrics in ILAMB, which translate model simulated NEE

652   into atmospheric CO_2 signal using an atmospheric transport model (Collier et al., 2018), is

653   intended for the evaluation of this sensitivity. The inferred atmospheric CO_2 concentration

654   from ELM v1 is very reasonable compared with observed NOAA flask data (Fig. S8 and S9).

655

656   **4.4. Model estimated carbon, nitrogen, and phosphorus pools and fluxes**

657   Global C, N, and P pools in our ELMv1-CNP simulation are in good agreement with

658   recent independent global estimates, indicating that ELMv1-CNP is capable of simulating

659   the contemporary C, N and P cycles. In Yang et al. (2019) it was shown that introduction of

660   more realistic mortality processes improved the model representation of longitudinal

661   spatial patterns of biomass across the Amazon basin. Here we show that an overall high

662   bias in biomass production is corrected through limits of vegetation production in response

663   to P availability, without compromising the improved spatial gradients obtained through

664   the mortality mechanism. It is worth mentioning that our understanding of nutrient stocks

665   and fluxes is much less advanced in comparison with the global C cycle. This has been

666   increasingly acknowledged for the global N cycle as increasing numbers of land surface

667   models have incorporated N cycle dynamics and C-N interactions (Zaehle et al., 2010;

668   Wieder et al., 2019; Davies-Barnard et al., 2020; Smith et al., 2014; Sellar et al., 2019; Goll

669   et al., 2017a; Gerber et al., 2010). Biological N fixation and N-use efficiency have been

670   identified as the key processes that need to be better constrained for land surface models

671   (Davies-Barnard et al., 2020).

672   Our understanding of P stocks and fluxes are even less advanced than that for the N

673   cycle, as shown in this study and other modeling studies that include P as a limiting

674   nutrient. This is mainly due to: (1) various forms of P with different level of availability for

675   plants and microbes, (2) geochemical processes in conjunction with biological processes

676   controlling P availability, and (3) technical challenges in measuring soil P. For example,

677   Hedley fractionation data provide a comprehensive picture of different P forms in soils and

678   has been used for model evaluation and/or initialization in all the land surface models that

679   include a prognostic phosphorus cycle (Wang et al., 2010; Goll et al., 2012; Yang et al.,

680   2014; Yang et al., 2019). However, this extraction method is time-consuming and

681   challenging, and not many routine measurements have been made using this technique.

682   As such, observational estimates of P pools and fluxes are extremely limited. Although

683   recent global Hedley database development (Yang and Post, 2011; Hou et al., 2018) has

684   been helpful in global model development and evaluation, more observational data on P

685   stocks and fluxes are needed to better constrain P-enabled models.

686

687

688   **4.5. Effects of accounting for the P cycle dynamics on simulated carbon balance**

689   **4.5.1. Spatial variation of nutrient limitation**

690   Our simulated nutrient limitation pattern broadly agrees with the findings from Elser et

691   al. (2007) which supports the generally accepted notion that tropical ecosystems residing

692   on highly weathered soils are P limited (Walker and Syers, 1976; Lebauer and Treseder,

693   2008). A recent study that predicted spatial patterns of N and P limitation using the ratios

694   of leaf N and P resorption efficiencies also found a shift from P limitation to N limitation

695   with increasing latitude (Du et al., 2020). Lebauer and Treseder (2008) showed that N

696   limitation is widespread, even in tropical regions. This is consistent with our model

697   simulations which show that although P is more limiting in tropical forests, N is also a

698   limiting nutrient. The geographic distribution of nutrient limitation is generally in

699   agreement with that from Goll et al. (2012) and Wang et al. (2010). Goll et al. (2012)

700   suggests that P limits C uptake mainly in low latitude regions and high latitudes, while N is

701   the limiting nutrient in temperate regions. It is worth mentioning that in Goll et al. (2012) N

702   and P limitation generally have distinct geographic occurrence while this study suggests NP

703   co-limitation occurs in many parts of the world. Wang et al. (2010) also showed that

704   productivity in tropical forests and savanna is limiting by P, while most other biomes are

705   limited by N. This is broadly consistent with our results but with a few key differences.

706   Wang et al. (2010) suggests that P is the limiting nutrient for savannas, whereas our results

707   show savannas are more limited by N. This may have to do with the lack of representation

708   of fire disturbance in Wang et al. (2010). Savannas are subject to regular wildfires, which

709   could have significant effects on nutrient cycle dynamics and nutrient limitation. For

710   example, it has been suggested that while combustion causes significant gaseous losses of

711   N from burned ecosystems, P is largely retained as ash (Herbert et al., 2003). Braakhekke et

712   al (2017) also showed that there are strong losses of N due to fire. Furthermore, Wang et

713   al. (2010) suggested that tropical forests are limited only by P, not by N, whereas our

714   results indicate that N and P both limit tropical forest productivity, although P limitation is

715   more dominant in most of the lowland tropical forests. This is consistent with a recent

716   meta-analysis of nutrient fertilization experiments in tropical forests (Wright et al., 2018).

717

718   **4.5.2. The implications for global carbon cycle and climate**

719   Historical C accumulation is a result of many complex and sometimes counteracting

720   processes controlling C fluxes and stocks (Lawrence et al., 2019), including accumulation of

721   carbon on land due to CO_2 fertilization, accumulation due to nitrogen deposition, carbon

722   fluxes due to climate variability and climate change, and losses and gains due to land cover

723   conversion and regrowth following historical land cover changes (LULCC fluxes).Over the

724   long term, two of the dominant processes controlling C accumulation in terrestrial

725   ecosystems are C emissions due to LULCC and C uptake due to the CO_2 fertilization effect. P

726   cycle dynamics have important impacts on both of these processes, but with opposite sign.

727   Globally, considering P cycle dynamics leads to lower carbon emissions associated with

728   deforestation by about 11% (161.21 Pg in CN vs 143.89 in CNP). Conversely, CO_2

729   fertilization at the global scale is reduced by 20% when P limitation is included during the

730   historical time period (134 Pg C vs 108 Pg C). In general, the ELMv1-CN simulation shows a

731   CO_2 fertilization effect on biomass that is too strong, which leads to a stronger than

732   observed carbon sink compared to observational constraints from both Hoffman et al.

733   (2014) and Le Quere et al. (2016). ELMv1-CN simulation also produces stronger carbon

734   emissions from LULCC due to having higher biomass compared to ELMv1-CNP. The CO_2

735   fertilization effect in the ELMv1-CN simulations is strong enough to overcome the LULCC

736   losses with the net result being too large of a sink throughout the historical time period for

737   the CN model. Both model configurations lose carbon too slowly due to LULCC in the period

738   from 1850–1940, when compared to the Hoffman et al. (2014) global estimate. Both

739   models also predict continued losses over the period 1940–1965, while the Hoffman et al.

740   (2014) estimate switches from net carbon loss to net carbon accumulation around 1940.

741   These are clearly shown in Fig. S7, which shows the time series of simulated change in land

742   carbon storage in response to changes in CO_2, LULCC, N deposition, and climate during

743   1850-2010. The ELMv1-CN and ELMv1-CNP models are similar to many other CMIP6

744   models with respect to this bias in the timing of transition from net land carbon source to

745   net land sink as shown in our ILAMB analysis of other land models in CMIP6.

746

747   We also note that, over the historical time period, P became more limiting as simulated

748   historical C accumulations became increasingly divergent between CN and CNP simulations.

749   This is mainly caused by stimulated plant productivity under higher atmospheric CO_2, which

750   leads to higher plant demand for P that is not balanced by increased supply of newly

751   mineralized P from the soil. This is consistent with other global modeling studies with

752   explicit representation of P cycle dynamics (Goll et al., 2012; Zhang et al., 2014), as well as

753   diagnostic studies that evaluated how CO_2 fertilization simulated by CMIP5 models could

754   be constrained by soil P availability using a mass balance approach (Wieder et al., 2015b;

755   Sun et al., 2017). Taken together, the limiting effect of P availability on C uptake will likely

756   have substantial consequences for projections of future C uptake.

757

758

759   **4.6. Limitations and future development**

760   While the ELMv1-CNP simulations presented here show that the model is capable of

761   representing contemporary C, N and P stocks and fluxes and capturing the observed

762   ecosystem responses to changes in atmospheric CO_2, the current configuration does have

763   limitations.

764   While the model represents disturbances such as fire and the interactions between

765   disturbances and nutrient cycle dynamics, these interactions and how they affect carbon

766   cycle processes have not been well constrained with observational data. There is a growing

767   body of literature investigating the biogeochemical signature of fire. For example, a meta-

768   analysis by Butler et al. (2018) shows that fire led to significantly higher concentration of

769   soil mineral P and lower soil and litter C:P and N:P ratios, therefore decoupling the P cycle

770   from the C and N cycles. We will take advantage of these recent findings to improve model

771   fidelity on this front.

772   Another area that needs to be improved is the treatment of N fixation and how that is

773   linked to P availability. N fixation in ELMv1-CNP is represented as a function of NPP

774   (Cleveland et al., 1999). While providing a reasonable global estimate of N fixation, the

775   approach ignores existing mechanistic understanding of nitrogen fixation processes

776   (Wieder et al., 2015a). Furthermore, several lines of evidence suggest that both symbiotic

777   and free-living N fixation rates depend on the availability of other elements, such as P and

778   molybdenum (Reed et al., 2013; Nasto et al., 2014). N fixation could have important

779   implications for the spatial distribution of N limitation vs P limitation. In the future we plan

780   to have a more mechanistic representation of N fixation in ELM.

781   In ELMv1-CNP, P limitation is represented by downregulating plant growth when P

782   demand is greater than soil P availability. The mechanisms by which P fundamentally limits

783   ecosystem productivity remain uncertain (Jiang et al., 2019). Some studies proposed that

784   there are linear or log-linear relationships between leaf P concentration and

785   photosynthetic parameters, although the relationship has been shown to be weak (Walker

786   et al., 2014). P fertilization experiments in P limited ecosystems do not support this

787   proposed relationship. A P fertilization experiment on highly weathered soils in Australia

788   showed that although leaf P concentration increased significantly (+50%) compared to

789   unfertilized trees, photosynthetic capacity was unaffected (Crous et al., 2015).

790   Another fertilization experiment in Hawaii showed that the increase of aboveground NPP

791   with P fertilization was caused mainly by increases in LAI instead of photosynthesis per unit

792   leaf area (Herbert and Fownes, 1995). Further laboratory and field experiments are needed

793   to help us better understand and represent the role of P in photosynthesis. Investigating

794   the detailed mechanisms through which leaf P concentration affects photosynthesis is an

795   active field of research (Jiang et al., 2019; Norby et al., 2017; Crous et al., 2015), and

796   representing these relationships in land models remains an outstanding challenge.

797   Uncertainty also remains regarding the ELMv1-CNP representation of sorption dynamics

798   and biochemical mineralization and their responses to changes in atmospheric CO_2 and

799   climate (Fleischer et al., 2019). Motivated by our previous modeling studies, several recent

800   field studies have started focusing on improving our mechanistic understanding and

801   providing quantitative relationships for modelling these processes (Cabugao et al., 2017;

802   Brenner et al., 2019). A recent study that upscaled site-measurements of potential

803   phosphatase activity to continental Europe using machine learning technique provides a

804   potential pathway toward generating benchmark data for biochemical mineralization on

805   regional to global scale (Sun et al., 2020). There are other mechanisms that could sustain

806   productivity with increasing P limitation but were not considered in ELMv1-CNP, such as

807   flexible stoichiometry and dynamic allocation. These will be investigated further in future

808   versions of E3SM. However, as Fleischer et al. (2019) pointed out, since plant N:P ratios in

809   highly P limited tropical forests are already at the high end of the observed spectrum, the

810   role of stoichiometry plasticity in sustaining tropical productivity could be limited.

811   While the representation of NSC has helped ELMv1-CNP to capture the interannual

812   variability of atmospheric CO_2 and to generate ecosystem responses to elevated CO_2

813   consistent with FACE measurements, the sizes and turnover times of NSC pools are not well

814   constrained. We will synthesize limited measurements on NSC from literature that include

815   observational and experimental data as well as measurements from isotopic studies to

816   better understand the dynamics of the NSC pool and to evaluate and refine its

817   representation in ELM. We also advocate for more measurements on NSC and how they

818   respond to environmental changes in diverse ecosystems to have a more complete

819   understanding and quantification of NSC.

820   Finally, although models such as ELMv1-CNP and CLM5 perform similarly when

821   evaluated against present-day metrics as gathered in ILAMB, we expect that the

822   differences among models in their representation of observed processes and in their

823   assumptions about how changes in atmospheric composition and climate will impact

824   ecosystem processes will lead to diverging predictions under future climate scenarios. We

825   will explore those differences and their consequences in future work.

826

827   **5. Conclusions**

828   In this study, we provide an evaluation of ELMv1-CNP using the ILAMB benchmarking

829   system, comparison with CO_2 manipulation experiments, and comparison with other

830   observational and modeling studies. Benchmarking with ILAMB indicates ELMv1-CNP

831   produces realistic estimates of present-day carbon pools and fluxes. Compared to a

832   simulation with optimal P availability, ELMv1-CNP produces better performance,

833   particularly for the metrics that are most relevant to land-atmosphere exchange. Our

834   results from CO_2 manipulation experiments suggest that ELMv1-CNP is able to capture

835   observed responses to elevated CO_2, including those for GPP, NPP, vegetation C, and LAI.

836   Further analysis suggests that the introduction of a non-structural carbon pool in ELMv1-

837   CNP is largely responsible for these improvements. Evaluating global C, N, and P pools and

838   fluxes in the context of literature values suggests that ELMv1-CNP provides a reasonable

839   representation of contemporary global scale C, N and P cycles.

840   We highlight the data needs for global land model evaluation, particularly the need for

841   more synthesis datasets on nutrient pools and fluxes, as well as observations from

842   manipulation experiments that provide additional benchmark data for nutrient cycle

843   evaluation. This need is becoming increasingly pressing as more land models are including N

844   and P cycle dynamics and C-N-P interactions. We also identify challenges in constraining P

845   cycle dynamics and point to the need for soil P measurements.

846   Our simulations suggest, probably not surprisingly, that in general P is the more limiting

847   nutrient in the tropical regions while N is more limiting in the middle to high latitudes.

848   However, our results also suggest widespread N and P colimitation, even in the tropical

849   regions where P limitation is more dominant. Our results show that C sources and sinks are

850   significantly affected by P limitation, as the historical CO2 fertilization effect was reduced by

851   20% and C emission due to LULCC was 11% lower when P limitation was considered. We

852   conclude that introduction of P cycle dynamics and C-N-P coupling will likely have

853   substantial consequences for projections of future C uptake.

854

855   Acknowledgement:

856 This research was supported as part of the Energy Exascale Earth System Model (E3SM) project,
857 funded by the U.S. Department of Energy, Office of Science, Office of Biological and
858 Environmental Research. This research was also supported by the Oak Ridge National
859 Laboratory's (ORNL) Terrestrial Ecosystem Science Focus Area (TES SFA). F. M. Hoffman was
860 supported by the Reducing Uncertainties in Biogeochemical Interactions through Synthesis and
861 Computation Scientific Focus Area (RUBISCO SFA), which is sponsored by the Regional and
862 Global Model Analysis (RGMA) Program in the Climate and Environmental Sciences Division
863 (CESD) of the Office of Biological and Environmental Research (BER) in the U.S. Department of
864 Energy Office of Science. We thank Min Xu for his help in running ILAMB. The E3SM model can
865 be accessed at https://www.osti.gov/doecode/biblio/10475 (doi:
866 10.11578/E3SM/dc.20180418.36). The input data is available at
867 https://web.lcrc.anl.gov/public/e3sm/inputdata/.
868 The model outputs used in this study can be downloaded at the website:
869 https://doi.org/10.6084/m9.figshare.12021348.

870

871

872   References:

873 Ainsworth, E. A. and Long, S. P.: What have we learned from 15 years of free-air CO2
874 enrichment (FACE)? A meta-analytic review of the responses of photosynthesis, canopy
875 properties and plant production to rising CO2, New phytologist, 165, 351-372, 2005.
876 Arora, V. K., Boer, G. J., Friedlingstein, P., Eby, M., Jones, C. D., Christian, J. R., Bonan, G.,
877 Bopp, L., Brovkin, V., and Cadule, P.: Carbon–concentration and carbon–climate feedbacks in
878 CMIP5 Earth system models, Journal of Climate, 26, 5289-5314, 2013.
879 Arora, V. K., Katavouta, A., Williams, R. G., Jones, C. D., Brovkin, V., Friedlingstein, P.,
880 Schwinger, J., Bopp, L., Boucher, O., and Cadule, P.: Carbon–concentration and carbon–climate
881 feedbacks in CMIP6 models and their comparison to CMIP5 models, Biogeosciences, 17, 4173-
882 4222, 2020.
883 Avitabile, V., Herold, M., Heuvelink, G. B., Lewis, S. L., Phillips, O. L., Asner, G. P., Armston,
884 J., Ashton, P. S., Banin, L., and Bayol, N.: An integrated pan-tropical biomass map using
885 multiple reference datasets, Global change biology, 22, 1406-1420, 2016.
886 Baig, S., Medlyn, B. E., Mercado, L. M., and Zaehle, S.: Does the growth response of woody
887 plants to elevated CO 2 increase with temperature? A model-oriented meta-analysis, Global
888 change biology, 21, 4303-4319, 2015.
889 Barron, A. R., Wurzburger, N., Bellenger, J. P., Wright, S. J., Kraepiel, A. M., and Hedin, L. O.:
890 Molybdenum limitation of asymbiotic nitrogen fixation in tropical forest soils, Nature
891 Geoscience, 2, 42-45, 2008.

892 Batjes, N. H.: Total carbon and nitrogen in the soils of the world, European journal of soil
893 science, 65, 10-21, 2014.
894 Beer, C., Reichstein, M., Tomelleri, E., Ciais, P., Jung, M., Carvalhais, N., Rödenbeck, C.,
895 Arain, M. A., Baldocchi, D., and Bonan, G. B.: Terrestrial gross carbon dioxide uptake: global
896 distribution and covariation with climate, Science, 329, 834-838, 2010.
897 Bonan, G. B., Lombardozzi, D. L., Wieder, W. R., Oleson, K. W., Lawrence, D. M., Hoffman, F.
898 M., and Collier, N.: Model structure and climate data uncertainty in historical simulations of the
899 terrestrial carbon cycle (1850–2014), Global Biogeochemical Cycles, 33, 1310-1326, 2019.
900 Bonan, G. B., Lawrence, P. J., Oleson, K. W., Levis, S., Jung, M., Reichstein, M., Lawrence, D.
901 M., and Swenson, S. C.: Improving canopy processes in the Community Land Model version 4
902 (CLM4) using global flux fields empirically inferred from FLUXNET data, Journal of
903 Geophysical Research: Biogeosciences, 116, 2011.
904 Brenner, J., Porter, W., Phillips, J. R., Childs, J., Yang, X., and Mayes, M. A.: Phosphorus
905 sorption on tropical soils with relevance to Earth system model needs, Soil research, 57, 17-27,
906 2019.
907 Burrows, S., Maltrud, M., Yang, X., Zhu, Q., Jeffery, N., Shi, X., Ricciuto, D., Wang, S., Bisht,
908 G., and Tang, J.: The DOE E3SM v1. 1 Biogeochemistry Configuration: Description and
909 Simulated Ecosystem-Climate Responses to Historical Changes in Forcing, Journal of Advances
910 in Modeling Earth Systems, 12, e2019MS001766, 2020.
911 Butler, O. M., Elser, J. J., Lewis, T., Mackey, B., and Chen, C.: The phosphorus-rich signature of
912 fire in the soil–plant system: a global meta-analysis, Ecology letters, 21, 335-344, 2018.
913 Cabugao, K. G., Timm, C. M., Carrell, A. A., Childs, J., Lu, T.-Y. S., Pelletier, D. A., Weston,
914 D. J., and Norby, R. J.: Root and rhizosphere bacterial phosphatase activity varies with tree
915 species and soil phosphorus availability in Puerto Rico tropical forest, Frontiers in plant science,
916 8, 1834, 2017.
917 Campbell, J., Berry, J., Seibt, U., Smith, S. J., Montzka, S., Launois, T., Belviso, S., Bopp, L.,
918 and Laine, M.: Large historical growth in global terrestrial gross primary production, Nature,
919 544, 84-87, 2017.
920 Cleveland, C., Townsend, A., Schimel, D., Fisher, H., Howarth, R., Hedin, L., Perakis, S., Latty,
921 E., Von Fischer, J., and Elseroad, A.: Global patterns of terrestrial biological nitrogen (N2)
922 fixation in natural ecosystems, Global Biogeochemical Cycles, 13, 623-645, 1999.
923 Collier, N., Hoffman, F. M., Lawrence, D. M., Keppel-Aleks, G., Koven, C. D., Riley, W. J.,
924 Mu, M., and Randerson, J. T.: The International Land Model Benchmarking (ILAMB) system:
925 design, theory, and implementation, Journal of Advances in Modeling Earth Systems, 10, 2731-
926 2754, 2018.
927 Crews, T. E., Farrington, H., and Vitousek, P. M.: Changes in asymbiotic, heterotrophic nitrogen
928 fixation on leaf litter of Metrosideros polymorpha with long-term ecosystem development in
929 Hawaii, Ecosystems, 3, 386-395, 2000.
930 Crous, K. Y., Osvaldsson, A., and Ellsworth, D. S.: Is phosphorus limiting in a mature
931 Eucalyptus woodland? Phosphorus fertilisation stimulates stem growth, Plant and soil, 391, 293-
932 305, 2015.
933 Davies-Barnard, T. and Friedlingstein, P.: The Global Distribution of Biological Nitrogen
934 Fixation in Terrestrial Natural Ecosystems, Global Biogeochemical Cycles, 34,
935 e2019GB006387, 10.1029/2019gb006387, 2020.

936   Davies-Barnard, T., Meyerholt, J., Zaehle, S., Friedlingstein, P., Brovkin, V., Fan, Y., Fisher, R.
937   A., Jones, C. D., Lee, H., and Peano, D.: Nitrogen cycling in CMIP6 land surface models:
938   Progress and limitations, Biogeosciences Discussions, 2020.
939   DeFries, R., Field, C., Fung, I., Collatz, G., and Bounoua, L.: Combining satellite data and
940   biogeochemical models to estimate global effects of human-induced land cover change on
941   carbon emissions and primary productivity, Global biogeochemical cycles, 13, 803-815, 1999.
942   Du, E., Terrer, C., Pellegrini, A. F., Ahlström, A., van Lissa, C. J., Zhao, X., Xia, N., Wu, X.,
943   and Jackson, R. B.: Global patterns of terrestrial nitrogen and phosphorus limitation, Nature
944   Geoscience, 13, 221-226, 2020.
945   Duarte, H. F., Raczka, B. M., Ricciuto, D. M., Lin, J. C., Koven, C. D., Thornton, P. E.,
946   Bowling, D. R., Lai, C.-T., Bible, K. J., and Ehleringer, J. R.: Evaluating the Community Land
947   Model (CLM4. 5) at a coniferous forest site in northwestern United States using flux and carbon-
948   isotope measurements, Biogeosciences (Online), 14, 2017.
949   Edwards, E., McCaffery, S., and Evans, J.: Phosphorus availability and elevated CO_2 affect
950   biological nitrogen fixation and nutrient fluxes in a clover dominated sward, New Phytologist,
951   169, 157-167, 2006.
952   Ehlers, I., Augusti, A., Betson, T. R., Nilsson, M. B., Marshall, J. D., and Schleucher, J.:
953   Detecting long-term metabolic shifts using isotopomers: CO_2-driven suppression of
954   photorespiration in C3 plants over the 20th century, Proceedings of the National Academy of
955   Sciences, 112, 15585-15590, 2015.
956   Ellsworth, D. S., Anderson, I. C., Crous, K. Y., Cooke, J., Drake, J. E., Gherlenda, A. N.,
957   Gimeno, T. E., Macdonald, C. A., Medlyn, B. E., and Powell, J. R.: Elevated CO 2 does not
958   increase eucalypt forest productivity on a low-phosphorus soil, Nature Climate Change, 7, 279-
959   282, 2017.
960   Elser, J. J., Bracken, M. E. S., Cleland, E. E., Gruner, D. S., Harpole, W. S., Hillebrand, H.,
961   Ngai, J. T., Seabloom, E. W., Shurin, J. B., and Smith, J. E.: Global analysis of nitrogen and
962   phosphorus limitation of primary producers in freshwater, marine and terrestrial ecosystems,
963   Ecology Letters, 10, 1135-1142, 10.1111/j.1461-0248.2007.01113.x, 2007.
964   Erb, K.-H., Kastner, T., Plutzar, C., Bais, A. L. S., Carvalhais, N., Fetzel, T., Gingrich, S.,
965   Haberl, H., Lauk, C., and Niedertscheider, M.: Unexpectedly large impact of forest management
966   and grazing on global vegetation biomass, Nature, 553, 73-76, 2018.
967   Finzi, A. C., Norby, R. J., Calfapietra, C., Gallet-Budynek, A., Gielen, B., Holmes, W. E.,
968   Hoosbeek, M. R., Iversen, C. M., Jackson, R. B., and Kubiske, M. E.: Increases in nitrogen
969   uptake rather than nitrogen-use efficiency support higher rates of temperate forest productivity
970   under elevated CO_2, Proceedings of the National Academy of Sciences, 104, 14014-14019,
971   2007.
972   Fleischer, K., Rammig, A., De Kauwe, M. G., Walker, A. P., Domingues, T. F., Fuchslueger, L.,
973   Garcia, S., Goll, D. S., Grandis, A., and Jiang, M.: Amazon forest response to CO 2 fertilization
974   dependent on plant phosphorus acquisition, Nature Geoscience, 12, 736-741, 2019.
975   Friedlingstein, P., Jones, M., O'Sullivan, M., Andrew, R., Hauck, J., Peters, G., Peters, W.,
976   Pongratz, J., Sitch, S., and Le Quéré, C.: Global carbon budget 2019, Earth System Science Data,
977   11, 1783-1838, 2019.
978   Gerber, S., Hedin, L. O., Oppenheimer, M., Pacala, S. W., and Shevliakova, E.: Nitrogen cycling
979   and feedbacks in a global dynamic land model, Global Biogeochemical Cycles, 24, GB1001,
980   10.1029/2008gb003336, 2010.

981   Ghimire, B., Riley, W. J., Koven, C. D., Mu, M., and Randerson, J. T.: Representing leaf and
982   root physiological traits in CLM improves global carbon and nitrogen cycling predictions,
983   Journal of Advances in Modeling Earth Systems, 8, 598-613, 2016.
984   Goll, D., Winkler, A., Raddatz, T., Dong, N., Prentice, I., Ciais, P., and Brovkin, V.: Carbon–
985   nitrogen interactions in idealized simulations with JSBACH (version 3.10), Geosci. Model Dev.,
986   10, 2009–2030, 2017a.
987   Goll, D., Brovkin, V., Parida, B., Reick, C., Kattge, J., Reich, P., van Bodegom, P., and
988   Niinemets, U.: Nutrient limitation reduces land carbon uptake in simulations with a model of
989   combined carbon, nitrogen and phosphorus cycling, Biogeosciences, 9, 3547-3569, 2012.
990   Goll, D., Vuichard, N., Maignan, F., Jornet-Puig, A., Sardans, J., Violette, A., Peng, S., Sun, Y.,
991   Kvakic, M., and Guimberteau, M.: A representation of the phosphorus cycle for ORCHIDEE
992   (revision 4520), 2017b.
993   Haverd, V., Smith, B., Canadell, J. G., Cuntz, M., Mikaloff-Fletcher, S., Farquhar, G.,
994   Woodgate, W., Briggs, P. R., and Trudinger, C. M.: Higher than expected CO2 fertilization
995   inferred from leaf to global observations, Global change biology, 26, 2390-2402, 2020.
996   Herbert, D. A. and Fownes, J. H.: Phosphorus limitation of forest leaf area and net primary
997   production on a highly weathered soil, Biogeochemistry, 29, 223-235, 1995.
998   Herbert, D. A., Williams, M., and Rastetter, E. B.: A model analysis of N and P limitation on
999   carbon accumulation in Amazonian secondary forest after alternate land-use abandonment,
1000 Biogeochemistry, 65, 121-150, 2003.
1001 Hoffman, F., Koven, C., Keppel-Aleks, G., Lawrence, D., Riley, W., Randerson, J., Ahlström,
1002 A., Abramowitz, G., Baldocchi, D., and Best, M.: International land model benchmarking
1003 (ILAMB) 2016 Workshop Report, US Department of Energy, Office of Science, 10, 1330803,
1004 2017.
1005 Hoffman, F. M., Randerson, J. T., Arora, V. K., Bao, Q., Cadule, P., Ji, D., Jones, C. D.,
1006 Kawamiya, M., Khatiwala, S., and Lindsay, K.: Causes and implications of persistent
1007 atmospheric carbon dioxide biases in Earth System Models, Journal of Geophysical Research:
1008 Biogeosciences, 119, 141-162, 2014.
1009 Hou, E., Tan, X., Heenan, M., and Wen, D.: A global dataset of plant available and unavailable
1010 phosphorus in natural soils derived by Hedley method, Scientific data, 5, 180166, 2018.
1011 Hou, E., Luo, Y., Kuang, Y., Chen, C., Lu, X., Jiang, L., Luo, X., and Wen, D.: Global meta-
1012 analysis shows pervasive phosphorus limitation of aboveground plant production in natural
1013 terrestrial ecosystems, Nature Communications, 11, 1-9, 2020.
1014 Houghton, R. A.: The contemporary carbon cycle, Treatise on geochemistry, 8, 473-513, 2003.
1015 Houlton, B. Z., Wang, Y.-P., Vitousek, P. M., and Field, C. B.: A unifying framework for
1016 dinitrogen fixation in the terrestrial biosphere, Nature, 454, 327-330, 10.1038/nature07028,
1017 2008.
1018 Huete, A., Didan, K., Miura, T., Rodriguez, E. P., Gao, X., and Ferreira, L. G.: Overview of the
1019 radiometric and biophysical performance of the MODIS vegetation indices, Remote sensing of
1020 environment, 83, 195-213, 2002.
1021 Hungate, B. A., Dukes, J. S., Shaw, M. R., Luo, Y., and Field, C. B.: Nitrogen and climate
1022 change, Science, 302, 1512-1513, 2003.
1023 Hungate, B. A., Stiling, P. D., Dijkstra, P., Johnson, D. W., Ketterer, M. E., Hymus, G. J.,
1024 Hinkle, C. R., and Drake, B. G.: CO2 elicits long-term decline in nitrogen fixation, Science, 304,
1025 1291, 2004.
1026 Jahnke, R.: The phosphorus cycle, Global Biogeochemical Cycles, 301-315, 1992.

Jiang, M., Caldararu, S., Zaehle, S., Ellsworth, D. S., and Medlyn, B. E.: Towards a more physiological representation of vegetation phosphorus processes in land surface models, New Phytologist, 222, 1223-1229, 2019.

Jobbágy, E. G. and Jackson, R. B.: The vertical distribution of soil organic carbon and its relation to climate and vegetation, Ecological applications, 10, 423-436, 2000.

Joiner, J., Yoshida, Y., Zhang, Y., Duveiller, G., Jung, M., Lyapustin, A., Wang, Y., and Tucker, C. J.: Estimation of terrestrial global gross primary production (GPP) with satellite data-driven models and eddy covariance flux data, Remote Sensing, 10, 1346, 2018.

Jones, C. D., Arora, V., Friedlingstein, P., Bopp, L., Brovkin, V., Dunne, J., Graven, H., Hoffman, F., Ilyina, T., and John, J. G.: C4MIP–The coupled climate–carbon cycle model intercomparison project: Experimental protocol for CMIP6, Geoscientific Model Development, 9, 2853-2880, 2016.

Jung, C.-G., Shin, H.-J., Park, M.-J., Joh, H.-K., and Kim, S.-J.: Evaluation of MODIS Gross Primary Production (GPP) by Comparing with GPP from CO 2 Flux Data Measured in a Mixed Forest Area, Journal of the Korean Society of Agricultural Engineers, 53, 1-8, 2011.

Kobayashi, H. and Dye, D. G.: Atmospheric conditions for monitoring the long-term vegetation dynamics in the Amazon using normalized difference vegetation index, Remote Sensing of Environment, 97, 519-525, 2005.

Köchy, M., Hiederer, R., and Freibauer, A.: Global distribution of soil organic carbon–Part 1: Masses and frequency distributions of SOC stocks for the tropics, permafrost regions, wetlands, and the world, Soil, 1, 351-365, 2015.

Koven, C., Riley, W., Subin, Z., Tang, J., Torn, M., Collins, W., Bonan, G., Lawrence, D., and Swenson, S.: The effect of vertically resolved soil biogeochemistry and alternate soil C and N models on C dynamics of CLM4, Biogeosciences, 10, 7109, 2013.

Lawrence, D. M., Fisher, R. A., Koven, C. D., Oleson, K. W., Swenson, S. C., Bonan, G., Collier, N., Ghimire, B., van Kampenhout, L., and Kennedy, D.: The Community Land Model version 5: Description of new features, benchmarking, and impact of forcing uncertainty, Journal of Advances in Modeling Earth Systems, 2019.

Le Quéré, C., Andrew, R., Canadell, J. G., Sitch, S., Korsbakken, J. I., Peters, G. P., Manning, A. C., Boden, T. A., Tans, P. P., and Houghton, R. A.: Global carbon budget 2016, 2016.

Le Quéré, C., Andrew, R. M., Friedlingstein, P., Sitch, S., Hauck, J., Pongratz, J., Pickers, P. A., Korsbakken, J. I., Peters, G. P., and Canadell, J. G.: Global carbon budget 2018, Earth System Science Data, 10, 2141-2194, 2018.

LeBauer, D. S. and Treseder, K. K.: Nitrogen limitation of net primary productivity in terrestrial ecosystems is globally distributed, Ecology, 89, 371-379, 2008.

Lin, B.-L., Sakoda, A., Shibasaki, R., Goto, N., and Suzuki, M.: Modelling a global biogeochemical nitrogen cycle in terrestrial ecosystems, Ecological Modelling, 135, 89-110, 2000.

Luo, Y., Randerson, J. T., Friedlingstein, P., Hibbard, K., Hoffman, F., Huntzinger, D., Jones, C., Koven, C., Lawrence, D., and Li, D.: A framework for benchmarking land models, 2012.

Mao, J., Ricciuto, D. M., Thornton, P. E., Warren, J. M., King, A. W., Shi, X., Iversen, C. M., and Norby, R. J.: Evaluating the Community Land Model in a pine stand with shading manipulations and 13CO2 labeling, Biogeosciences (Online), 13, 2016.

Marklein, A. R. and Houlton, B. Z.: Nitrogen inputs accelerate phosphorus cycling rates across a wide variety of terrestrial ecosystems, New Phytologist, 193, 696-704, 2012.

1072   Matthews, E.: Global litter production, pools, and turnover times: Estimates from measurement
1073   data and regression models, Journal of Geophysical Research: Atmospheres, 102, 18771-18800,
1074   1997.
1075   McGill, W. and Cole, C.: Comparative aspects of cycling of organic C, N, S and P through soil
1076   organic matter, Geoderma, 26, 267-286, 1981.
1077   Melillo, J., Steudler, P., Aber, J., Newkirk, K., Lux, H., Bowles, F., Catricala, C., Magill, A.,
1078   Ahrens, T., and Morrisseau, S.: Soil warming and carbon-cycle feedbacks to the climate system,
1079   Science, 298, 2173-2176, 2002.
1080   Metcalfe, D. B., Ricciuto, D., Palmroth, S., Campbell, C., Hurry, V., Mao, J., Keel, S. G., Linder,
1081   S., Shi, X., and Näsholm, T.: Informing climate models with rapid chamber measurements of
1082   forest carbon uptake, Global change biology, 23, 2130-2139, 2017.
1083   Mitchard, E. T., Feldpausch, T. R., Brienen, R. J., Lopez-Gonzalez, G., Monteagudo, A., Baker,
1084   T. R., Lewis, S. L., Lloyd, J., Quesada, C. A., and Gloor, M.: Markedly divergent estimates of A
1085   mazon forest carbon density from ground plots and satellites, Global Ecology and Biogeography,
1086   23, 935-946, 2014.
1087   Nakhavali, M., Mercado, L. M., Hartley, I. P., Sitch, S., Cunha, F. V., di Ponzio, R., Lugli, L. F.,
1088   Quesada, C. A., Andersen, K. M., and Chadburn, S. E.: Representation of phosphorus cycle in
1089   Joint UK Land Environment Simulator (vn5. 5_JULES-CNP), Geoscientific Model
1090   Development Discussions, 1-24, 2021.
1091   Nasto, M. K., Alvarez-Clare, S., Lekberg, Y., Sullivan, B. W., Townsend, A. R., and Cleveland,
1092   C. C.: Interactions among nitrogen fixation and soil phosphorus acquisition strategies in lowland
1093   tropical rain forests, Ecology Letters, 17, 1282-1289, 2014.
1094   Norby, R. J., Gu, L., Haworth, I. C., Jensen, A. M., Turner, B. L., Walker, A. P., Warren, J. M.,
1095   Weston, D. J., Xu, C., and Winter, K.: Informing models through empirical relationships
1096   between foliar phosphorus, nitrogen and photosynthesis across diverse woody species in tropical
1097   forests of Panama, New Phytologist, 215, 1425-1437, 2017.
1098   Olander, L. P. and Vitousek, P. M.: Regulation of soil phosphatase and chitinase activityby N
1099   and P availability, Biogeochemistry, 49, 175-191, 2000.
1100   Oleson, K., Lawrence, D., Bonan, G., Drewniak, B., Huang, M., Koven, C., Levis, S., Li, F.,
1101   Riley, W., and Subin, Z.: Technical Description of version 4.5 of the Community Land Model
1102   (CLM)(NCAR Technical Note No. NCAR/TN-503+ STR). Citeseer, National Center for
1103   Atmospheric Research, PO Box, 3000, 2013.
1104   Pan, Y., Birdsey, R. A., Fang, J., Houghton, R., Kauppi, P. E., Kurz, W. A., Phillips, O. L.,
1105   Shvidenko, A., Lewis, S. L., and Canadell, J. G.: A large and persistent carbon sink in the
1106   world‚Äôs forests, Science, 333, 988-993, 2011.
1107   Post, W. M., Pastor, J., Zinke, P. J., and Stangenberger, A. G.: Global patterns of soil nitrogen
1108   storage, Nature, 317, 613-616, 1985.
1109   Raczka, B., Duarte, H. F., Koven, C. D., Ricciuto, D., Thornton, P. E., Lin, J. C., and Bowling,
1110   D. R.: An observational constraint on stomatal function in forests: evaluating coupled carbon and
1111   water vapor exchange with carbon isotopes in the Community Land Model (CLM4. 5),
1112   Biogeosciences, 13, 5183-5204, 2016.
1113   Reed, S. C., Cleveland, C. C., and Townsend, A. R.: Relationships among phosphorus,
1114   molybdenum and free-living nitrogen fixation in tropical rain forests: results from observational
1115   and experimental analyses, Biogeochemistry, 1-13, 2013.
1116   Reed, S. C., Yang, X., and Thornton, P. E.: Incorporating phosphorus cycling into global
1117   modeling efforts: a worthwhile, tractable endeavor, New Phytologist, 208, 324-329, 2015.

1118   Santoro, M., Beaudoin, A., Beer, C., Cartus, O., Fransson, J. E., Hall, R. J., Pathe, C.,
1119   Schmullius, C., Schepaschenko, D., and Shvidenko, A.: Forest growing stock volume of the
1120   northern hemisphere: Spatially explicit estimates for 2010 derived from Envisat ASAR, Remote
1121   Sensing of Environment, 168, 316-334, 2015.
1122   Sellar, A. A., Jones, C. G., Mulcahy, J., Tang, Y., Yool, A., Wiltshire, A., O'connor, F. M.,
1123   Stringer, M., Hill, R., and Palmieri, J.: UKESM1: Description and evaluation of the UK Earth
1124   System Model, Journal of Advances in Modeling Earth Systems, 2019.
1125   Shabanov, N. V., Huang, D., Yang, W., Tan, B., Knyazikhin, Y., Myneni, R. B., Ahl, D. E.,
1126   Gower, S. T., Huete, A. R., and Aragão, L. E. O.: Analysis and optimization of the MODIS leaf
1127   area index algorithm retrievals over broadleaf forests, IEEE Transactions on Geoscience and
1128   Remote Sensing, 43, 1855-1865, 2005.
1129   Smil, V.: P HOSPHORUS IN THE E NVIRONMENT: Natural Flows and Human Interferences,
1130   Annual review of energy and the environment, 25, 53-88, 2000.
1131   Smith, B., Warlind, D., Arneth, A., Hickler, T., Leadley, P., Siltberg, J., and Zaehle, S.:
1132   Implications of incorporating N cycling and N limitations on primary production in an
1133   individual-based dynamic vegetation model, Biogeosciences, 11, 2027-2054, 2014.
1134   Sun, Y., Goll, D. S., Ciais, P., Peng, S., Margalef, O., Asensio, D., Sardans, J., and Peñuelas, J.:
1135   Spatial pattern and environmental drivers of acid phosphatase activity in Europe, 2020.
1136   Sun, Y., Goll, D. S., Chang, J., Ciais, P., Guenet, B., Helfenstein, J., Huang, Y., Lauerwald, R.,
1137   Maignan, F., and Naipal, V.: Global evaluation of the nutrient-enabled version of the land
1138   surface model ORCHIDEE-CNP v1. 2 (r5986), Geoscientific Model Development, 14, 1987-
1139   2010, 2021.
1140   Sun, Y., Peng, S., Goll, D. S., Ciais, P., Guenet, B., Guimberteau, M., Hinsinger, P., Janssens, I.
1141   A., Peñuelas, J., and Piao, S.: Diagnosing phosphorus limitations in natural terrestrial ecosystems
1142   in carbon cycle models, Earth's future, 5, 730-749, 2017.
1143   Terrer, C., Jackson, R. B., Prentice, I. C., Keenan, T. F., Kaiser, C., Vicca, S., Fisher, J. B.,
1144   Reich, P. B., Stocker, B. D., and Hungate, B. A.: Nitrogen and phosphorus constrain the CO 2
1145   fertilization of global plant biomass, Nature Climate Change, 9, 684-689, 2019.
1146   Thornton, P., Doney, S., Lindsay, K., Moore, J., Mahowald, N., Randerson, J., Fung, I.,
1147   Lamarque, J., Feddema, J., and Lee, Y.: Carbon-nitrogen interactions regulate climate-carbon
1148   cycle feedbacks: results from an atmosphere-ocean general circulation model, 2009.
1149   Thornton, P. E., Lamarque, J.-F., Rosenbloom, N. A., and Mahowald, N. M.: Influence of
1150   carbon-nitrogen cycle coupling on land model response to CO2 fertilization and climate
1151   variability, Global Biogeochemical Cycles, 21, GB4018, 10.1029/2006gb002868, 2007.
1152   Thum, T., Caldararu, S., Engel, J., Kern, M., Pallandt, M., Schnur, R., Yu, L., and Zaehle, S.: A
1153   new terrestrial biosphere model with coupled carbon, nitrogen, and phosphorus cycles (QUINCY
1154   v1. 0; revision 1772), Geoscientific Model Development, 12, 4781-4802, 2019.
1155   Todd-Brown, K., Randerson, J., Post, W., Hoffman, F., Tarnocai, C., Schuur, E., and Allison, S.:
1156   Causes of variation in soil carbon simulations from CMIP5 Earth system models and comparison
1157   with observations, Biogeosciences, 10, 1717-1736, 2013.
1158   Treseder, K. K. and Vitousek, P. M.: Effects of soil nutrient availability on investment in
1159   acquisition of N and P in Hawaiian rain forests, Ecology, 82, 946-954, 2001.
1160   Van den Hurk, B., Kim, H., Krinner, G., Seneviratne, S. I., Derksen, C., Oki, T., Douville, H.,
1161   Colin, J., Ducharne, A., and Cheruy, F.: LS3MIP (v1. 0) contribution to CMIP6: the Land
1162   Surface, Snow and Soil moisture Model Intercomparison Project-aims, setup and expected
1163   outcome, Geoscientific Model Development, 9, 2809-2832, 2016.

1164 Vitousek, P. M., Menge, D. N., Reed, S. C., and Cleveland, C. C.: Biological nitrogen fixation:
1165 rates, patterns and ecological controls in terrestrial ecosystems, Philosophical Transactions of the
1166 Royal Society B: Biological Sciences, 368, 20130119, 2013.
1167 Vitousek, P. M., Porder, S., Houlton, B. Z., and Chadwick, O. A.: Terrestrial phosphorus
1168 limitation: mechanisms, implications, and nitrogen-phosphorus interactions, Ecological
1169 applications, 20, 5-15, 2010.
1170 Walker, A. P., Beckerman, A. P., Gu, L., Kattge, J., Cernusak, L. A., Domingues, T. F., Scales,
1171 J. C., Wohlfahrt, G., Wullschleger, S. D., and Woodward, F. I.: The relationship of leaf
1172 photosynthetic traits–Vcmax and Jmax–to leaf nitrogen, leaf phosphorus, and specific leaf area: a
1173 meta-analysis and modeling study, Ecology and evolution, 4, 3218-3235, 2014.
1174 Walker, T. and Syers, J.: The fate of phosphorus during pedogenesis, Geoderma, 15, 1-19, 1976.
1175 Wang, Y., Ciais, P., Goll, D. S., Huang, Y., Luo, Y., Wang, Y.-P., Bloom, A. A., Broquet, G.,
1176 Hartmann, J., and Peng, S.: GOLUM-CNP v1. 0: a data-driven modeling of carbon, nitrogen and
1177 phosphorus cycles in major terrestrial biomes, 2018.
1178 Wang, Y.-P., Law, R. M., and Pak, B.: A global model of carbon, nitrogen and phosphorus
1179 cycles for the terrestrial biosphere, Biogeosciences, 7, 2261-2282, 10.5194/bg-7-2261-2010,
1180 2010.
1181 Wang, Y. P., Houlton, B. Z., and Field, C. B.: A model of biogeochemical cycles of carbon,
1182 nitrogen, and phosphorus including symbiotic nitrogen fixation and phosphatase production,
1183 Global Biogeochemical Cycles, 21, GB1018, 10.1029/2006gb002797, 2007.
1184 Welp, L. R., Keeling, R. F., Meijer, H. A., Bollenbacher, A. F., Piper, S. C., Yoshimura, K.,
1185 Francey, R. J., Allison, C. E., and Wahlen, M.: Interannual variability in the oxygen isotopes of
1186 atmospheric CO 2 driven by El Niño, Nature, 477, 579-582, 2011.
1187 Wieder, W. R., Cleveland, C. C., Lawrence, D. M., and Bonan, G. B.: Effects of model structural
1188 uncertainty on carbon cycle projections: biological nitrogen fixation as a case study,
1189 Environmental Research Letters, 10, 044016, 2015a.
1190 Wieder, W. R., Cleveland, C. C., Smith, W. K., and Todd-Brown, K.: Future productivity and
1191 carbon storage limited by terrestrial nutrient availability, Nature Geoscience, 8, 441, 2015b.
1192 Wieder, W. R., Lawrence, D. M., Fisher, R. A., Bonan, G. B., Cheng, S. J., Goodale, C. L.,
1193 Grandy, A. S., Koven, C. D., Lombardozzi, D. L., and Oleson, K. W.: Beyond static
1194 benchmarking: Using experimental manipulations to evaluate land model assumptions, Global
1195 Biogeochemical Cycles, 33, 1289-1309, 2019.
1196 Wright, S. J., Turner, B. L., Yavitt, J. B., Harms, K. E., Kaspari, M., Tanner, E. V., Bujan, J.,
1197 Griffin, E. A., Mayor, J. R., and Pasquini, S. C.: Plant responses to fertilization experiments in
1198 lowland, species-rich, tropical forests, Ecology, 99, 1129-1138, 2018.
1199 Xu, R. I. and Prentice, I. C.: Terrestrial nitrogen cycle simulation with a dynamic global
1200 vegetation model, Global Change Biology, 14, 1745-1764, 10.1111/j.1365-2486.2008.01625.x,
1201 2008.
1202 Yang, X. and Post, W.: Phosphorus transformations as a function of pedogenesis: a synthesis of
1203 soil phosphorus data using Hedley fractionation method, Biogeosciences, 8, 2907-2916, 2011.
1204 Yang, X., Post, W., Thornton, P., and Jain, A.: The distribution of soil phosphorus for global
1205 biogeochemical modeling, Biogeosciences, 10, 2525-2537, 2013.
1206 Yang, X., Thornton, P., Ricciuto, D., and Post, W.: The role of phosphorus dynamics in tropical
1207 forests–a modeling study using CLM-CNP, Biogeosciences, 11, 1667-1681, 2014.

1208 Yang, X., Thornton, P. E., Ricciuto, D. M., and Hoffman, F. M.: Phosphorus feedbacks
1209 constraining tropical ecosystem responses to changes in atmospheric CO2 and climate,
1210 Geophysical Research Letters, 43, 7205-7214, 10.1002/2016GL069241, 2016.
1211 Yang, X., Wittig, V., Jain, A., and Post, W.: Integration of nitrogen cycle dynamics into the
1212 Integrated Science Assessment Model for the study of terrestrial ecosystem responses to global
1213 change, Global Biogeochemical Cycles, 23, 2009.
1214 Yang, X., Ricciuto, D. M., Thornton, P. E., Shi, X., Xu, M., Hoffman, F., and Norby, R. J.: The
1215 effects of phosphorus cycle dynamics on carbon sources and sinks in the Amazon region: a
1216 modeling study using ELM v1, Journal of Geophysical Research: Biogeosciences, 2019.
1217 Zaehle, S., Friend, A., Friedlingstein, P., Dentener, F., Peylin, P., and Schulz, M.: Carbon and
1218 nitrogen cycle dynamics in the O-CN land surface model: 2. Role of the nitrogen cycle in the
1219 historical terrestrial carbon balance, Global Biogeochemical Cycles, 24, 2010.
1220 Zhang, Q., Wang, Y.-P., Matear, R., Pitman, A., and Dai, Y.: Nitrogen and phosphorous
1221 limitations significantly reduce future allowable CO2 emissions, Geophysical Research Letters,
1222 41, 632-637, 2014.
1223 Zhu, Q., Riley, W. J., Tang, J., Collier, N., Hoffman, F. M., Yang, X., and Bisht, G.:
1224 Representing nitrogen, phosphorus, and carbon interactions in the E3SM land model:
1225 Development and global benchmarking, Journal of Advances in Modeling Earth Systems, 11,
1226 2238-2258, 2019.

1227

1228

1229

1230

1231

1232

1233

1234

1235

1236

1237

1238

1239

1240

1241

1242

1243
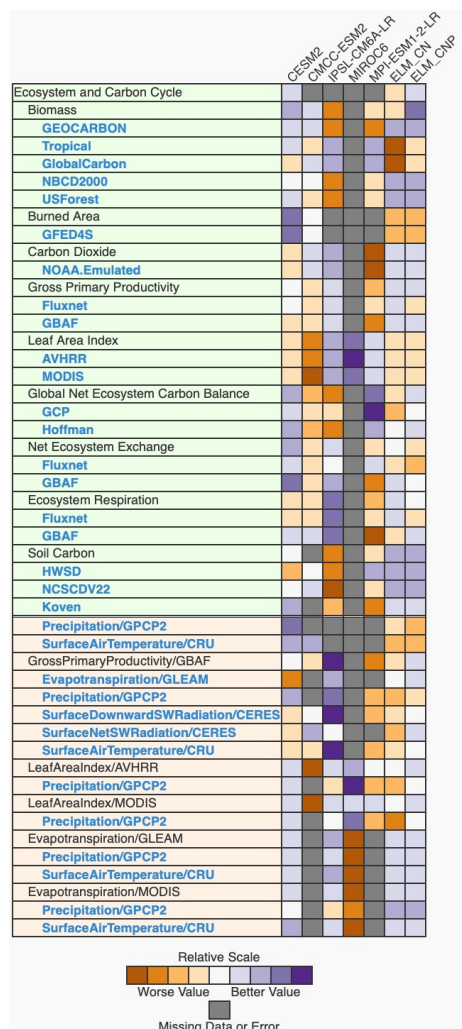
1244

1245

1246 Figure 1: ILAMB carbon cycle scores for ELMv1-CNP and ELM-CN and a few land models in

1247 CMIP6. Shown here is the relative score, indicating the performance of each model relative to

1248 other models. References for benchmarking data for each variable are provided in Table S4.

1249 Outputs for other land models are from the LS3MIP offline simulations archive in CMIP6. These

1250 simulations were performed using the same resolution and forcing data as this study. CLM4.5 is

1251 the land model in CMCC-ESM2. CLM5 is the land model for CESM2. OCHIDEE is the land model

1252 for IPSL. JABACH is the land model for MPP-ESM1.2. VISIT is the land model for MIROC6.
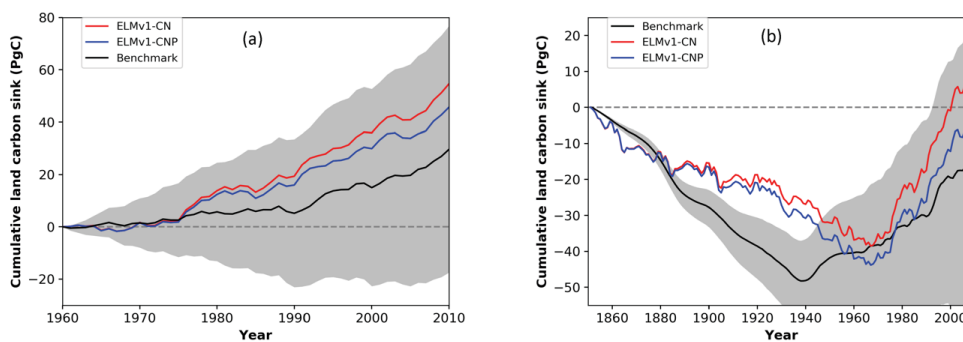
1253

1254 Figure 2: ELMv1-CNP and ELMv1-CN simulated global land carbon accumulation for the time

1255 period (a) 1960-2010 and (b) and 1850-2010. Benchmark data (black lines with uncertainty

1256 estimate in grey) are from (a) Global carbon project (Le Quere et al., 2016) and (b) Hoffman et

1257 al. (2014).

1258

1259

1260
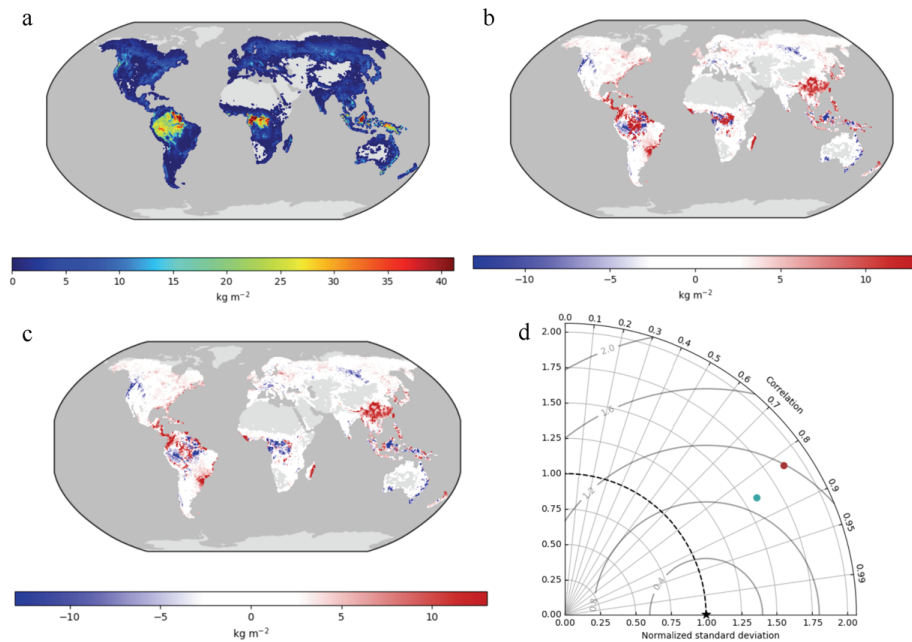
Figure 3: Global pattern of simulated biomass: (a) benchmark data, (b) ELMv1-CN bias (c)
ELMv1-CNP bias and (d) spatial Taylor diagram for model-benchmark comparison (red dot is for
ELMv1-CN and blue dot is for ELMv1-CNP). Benchmark data here is from the GEOCARBON
product (Saatchi et al.,2011).

1270
1271
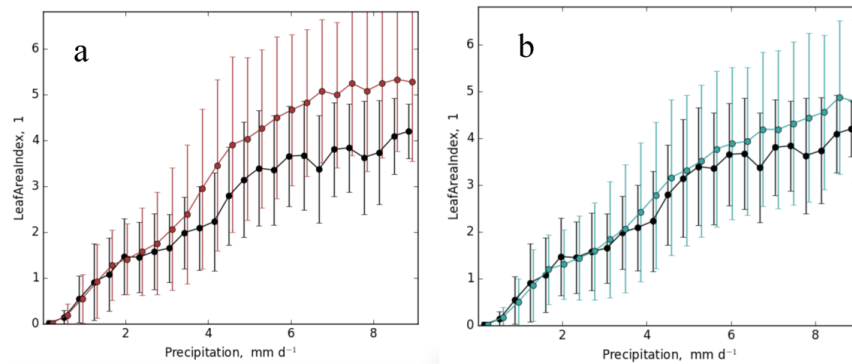
Figure 4: ILAMB relationship plot between LAI and climatological annual precipitation and (a)

ELMv1-CN (b) ELMv1-CNP. Black line is the observationally derived relationship. Error bars

indicate one standard derivation of LAI for all grid cells within the precipitation bin. Observed

LAI is from MODIS LAI product.

1272
1273
1274
1275

1276
1277
1278
1279
1280
1281
1282
1283
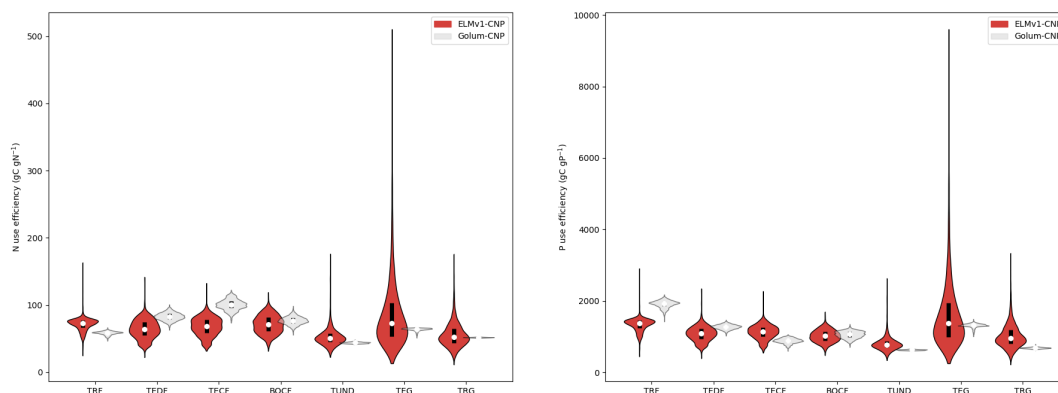
1284
1285
1286 Figure 5: Violin plots of nitrogen use efficiency (NUE) and phosphorus use efficiency (PUE) from

1287 ELMv1-CNP and GOLUM-CNP for seven biomes: tropical rainforest (TRF), temperate deciduous

1288 forest (TEDF), temperate coniferous forest (TECF), boreal coniferous forest (BOCF), temperate

1289 grassland (TEG) and tropical grassland (TRG). Plots show the medians of all grid cells in each

1290 biome (open circles) and the probability density distribution (balloons).

1291

1292

1293

1294
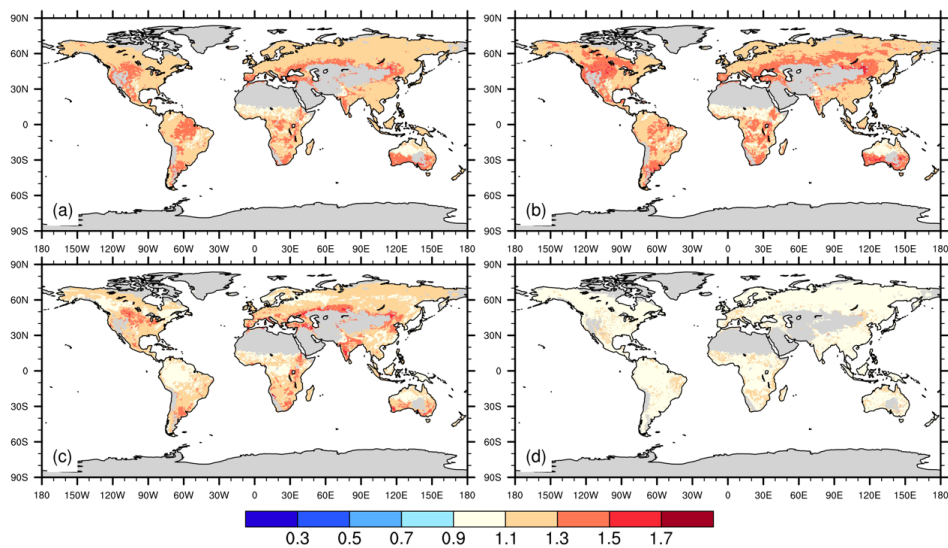
1295

1296

1297   Figure 6: Spatial distribution of the effect size of CO_2 enrichment on (a) GPP (b) NPP (c)

1298   Vegetation carbon (d) LAI. Effect sizes were calculated for each grid cell as the mean annual

1299   values of GPP, NPP, vegetation carbon and LAI from CO_2 enrichment simulation divided those

1300   from the control simulations between 2001-2010.

1301
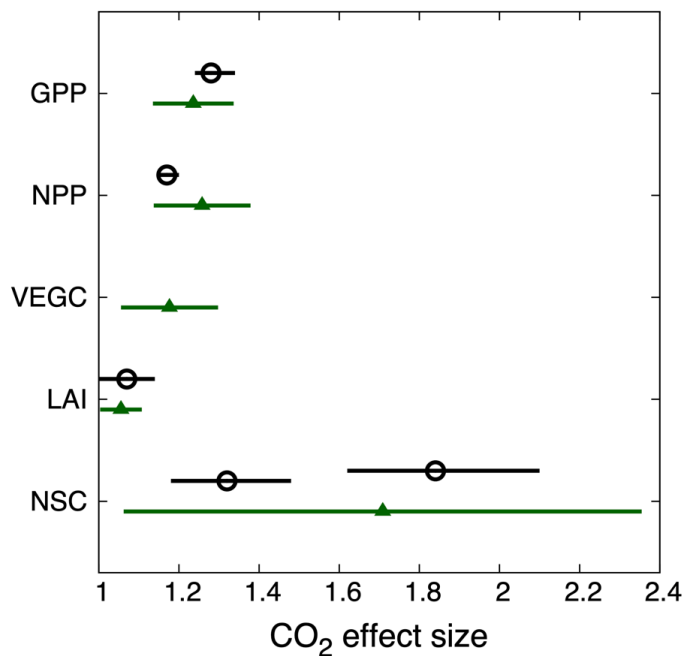
1302

1303   Figure 7: Observed (open circles) and simulated (solid circles) effect size of CO_2 enrichment on

1304   GPP, NPP, LAI, vegetation carbon and non-structural carbon. Observations show the mean

1305   ($\pm$95% confidence interval; Ainsworth and Long, 2005). There are two observations of NSC

1306   shown here, one is for sugar and the other is for starch, while model conceptualization of NSC

1307   includes both sugar and starch. Simulated responses show the global mean effect sizes ($\pm$ stand

1308   derivation; calculated to provide an estimate of spatial variation).

1309

1310
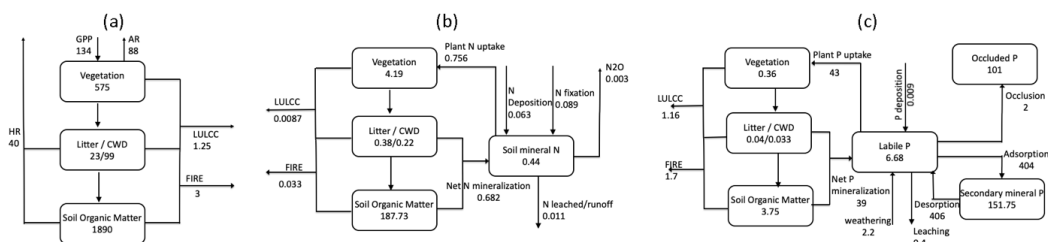
Figure 8: (left) terrestrial C cycle, (middle) N cycle, and (right) P cycle as simulated by ELMv1-CNP, shown here are mean values between between 2001-2010. Vegetation and soil C, N and P pools are in units of Pg C, Pg N and Pg P, respectively. C and N fluxes are given in Pg C yr^{-1} and Pg N yr^{-1}, and P fluxes are given in Tg P yr^{-1}.

1327
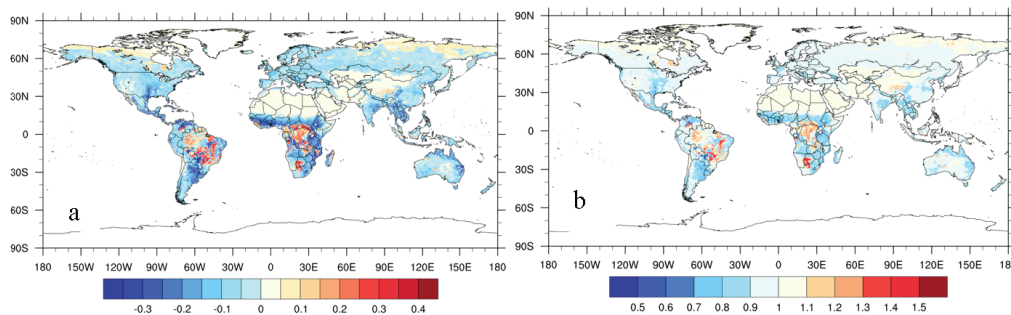
Figure 9: (a) Spatial variation of the extent of nutrient limitation on plant growth. Regions with
a negative value are more limited by N, while regions with a positive value are more limited by
P. Larger absolute values are associated with stronger limitation. Values plotted are the
proportion by which plant growth is reduced due to N limitation or P limitation: $1-f_P$ when f_P
$<f_N$ and f_N-1 when $f_N <f_P$, where f_P is the limitation factor on plant growth considering P
supply and demand, while f_N is the limitation factor on plant growth considering N supply and
demand (Yang *et al*., 2014). (b) Spatial variation of the ratios between P limitation and N
limitation indicating the degree of co-limitation. Values plotted are the ratios between f_N and
f_P: f_N/f_P. Regions with values less than 1 indicate more N limitation and regions with values
greater than 1 are more limited by P. Values close to 1 indicate NP co-limitation.

1338

1339
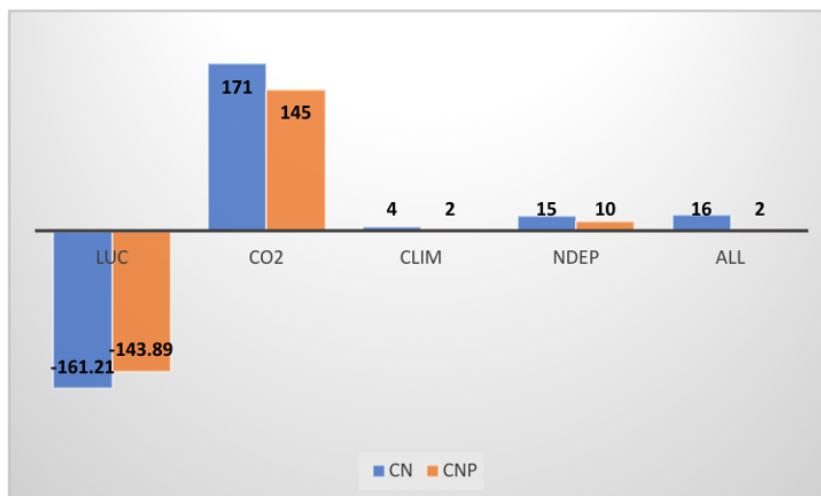
1340

Fig. 10: (a) Cumulative global carbon storage from 1850 to 2010 from ELMv1-CN and ELMv1-CNP simulations with changes in land use and land cover change (LUC), atmospheric CO_2 (CO_2), climate (CLIM), N deposition (NDEP), and all factor combined (ALL). These are calculated as the accumulation of NEE between 1850 and 2010 for the historical transient model simulations listed in Table 1.

1341
1342
1343
1344
1345
1346
1347
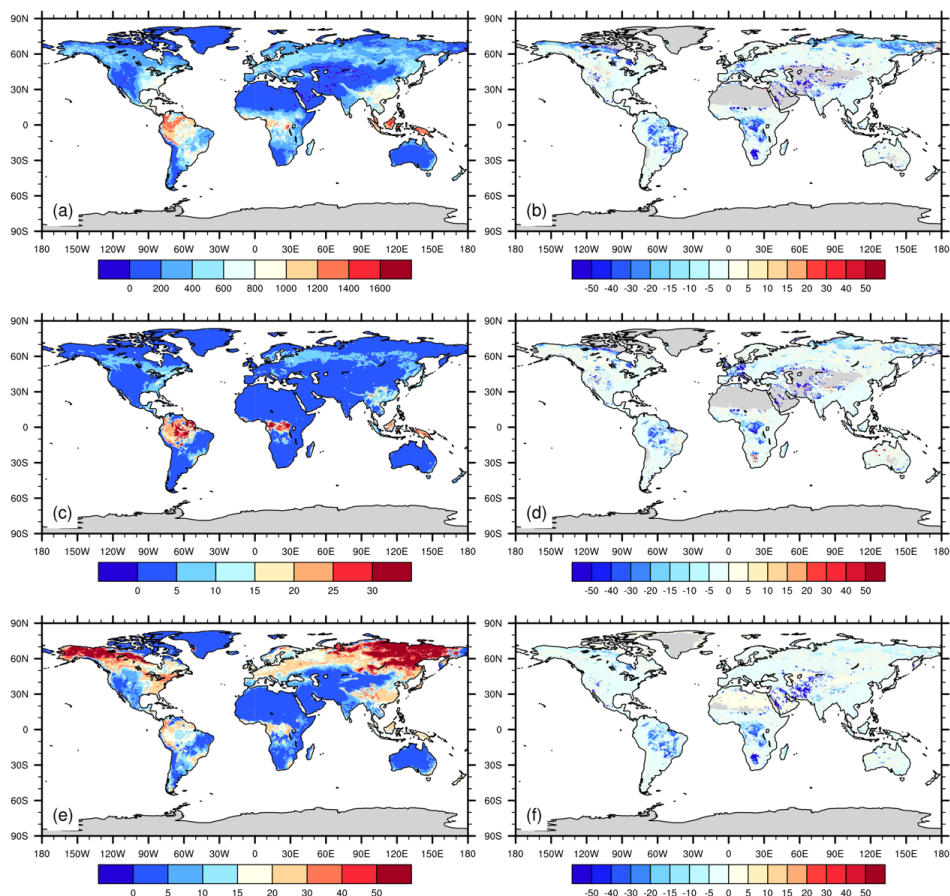
Fig. 11: Average estimates and effects of phosphorus dynamics on (a,b) net primary productivity, (c,d) vegetation carbon and (e,f) soil organic carbon for the years 2001-2010, as estimated by ELM v1. The effects of P dynamics are expressed as percentage deviation between CNP and CN configurations

1359
1360   Table 1: Summary of model simulations
1361

Experiment	P coupling	CO2 forcing	LULCC	Climate forcing	N depos
Ctrl_CN	off	1850	1850	steady state[a]	1850
Ctrl_CNP	on	1850	1850	steady state[a]	1850
Hist_CN_CO₂	off	transient	1850	steady state[a]	1850
Hist_CNP_CO₂	on	transient	1850	steady state[a]	1850
Hist_CN_LUC	off	1850	tranisient	steady state[a]	1850
Hist_CNP_LUC	on	1850	transient	steady state[a]	1850
Hist_CN_climate	off	1850	1850	transient[b]	1850
Hist_CNP_ climate	on	1850	1850	transient[b]	1850
Hist_CN_NDep	off	1850	1850	steady state[a]	transient
Hist_CNP_Ndep	on	1850	1850	steady state[a]	transient
Hist_CN_all	off	Transient	A d	transient[b]	transient
Hist_CNP_all	on	transient	transient	transient[b]	transient
FACE_CO₂	on	+200ppm (1991-2010)	transient	transient[b]	transient

1362   a Cycling of 20-year time series of GSWP3 reanalysis product (1901-1920)
1363   b Historical time series of GSWP3 reanalysis product (1901-2010)
1364
1365

1366

1367

1368

1369

1370

1371

1372

1373

1374

1375

1376

1377

1378

1379   Table 2: Comparison of ELMv1-CNP Simulated Mean Global Stocks and Fluxes of C, N and P

1380   between 2001 and 2010 to Observation-based Estimates

	ELMv1-CNP	Observation-based Estimates		
			Source	Methodology
GPP (Pg C yr^{-1})	134.15	123±8	Beer et al., 2010	Using eddy covariance flux data and various diagnostic models
		150-175	Welp et al., 2011	Based on oxygen isotopes of atmospheric CO_2
		119±6	Jung et al., 2011	upscaled FLUXNET observations to the global scale using the machine learning technique, model tree ensembles (MTE).
		121.60 - 129.42	Zhang et al., 2017	Light use efficiency theory, MODIS satellite data and climate data
		140	Joiner et al., 2018	Satellite Data-Driven Models and Eddy Covariance Flux Data
NPP (Pg C yr^{-1})	46.09	55±11	Turner et al., 2006	MODIS products
		33-49	Smith et al., 2016	MODIS NPP algorithm driven by long-term Global Inventory Modeling and Mapping Studies (GIMMS) FPAR and LAI data
Vegetation C (Pg C)	575.45	550±100	Houghton, 2003	Literature synthesis
		560±94	Defries et al., 1999	
Soil carbon (Pg C)	1890.78	1750±250	Houghton, 2003	Literature synthesis
		2344	Jobbagy and Jackson, 2000	based on >2700 soil profiles in three global databases supplemented with data for climate, vegetation, and land use.
		3000	Kochy et al., 2015	Based on the Harmonized World Soil Database(HWSD), but with more detailed estimates for permafrost and tropical wetland soil carbon
		2376–2456	Batjes, 2014	Top 2m. Based on 4353 soil profiles distributed globally and the FAO Soil Map of the World.
Top 1m soil carbon (Pg C)	1134.41	1462-1548	Batjes, 2014	Based on 4353 soil profiles distributed globally and the FAO Soil Map of the World.
		1325	Kochy et al., 2015	Based on the Harmonized World Soil Database(HWSD), but with more detailed estimates for permafrost and tropical wetland soil carbon
		1502	Jobbagy and Jackson, 2000	based on >2700 soil profiles in three global databases supplemented with

				data for climate, vegetation, and land use.
Soil organic N (Pg N)	188.79	95	Post et al. 1985	Based on 3100 soil profiles and a global map of Holdridge life zones
		133-140	Batjes et al., 2014	Top 1m. Based on 4353 soil profiles distributed globally and the FAO Soil Map of the World
N fixation (Tg N yr^{-1})	89	40-100	Vitousek et al., 2013	Estimates for Pre-industrial. Combining information on N fluxes with ^{15}N relative abundance data for terrestrial ecosystems
		52-130	Davies-Barnard and Friedlingstein (2020)	Based on a comprehensive meta-analysis of field measurements
N uptake (Tg N yr^{-1})	760	570	Wang et al., 2018	Data-driven estimates. Observations include observed stoichiometric ratios, N and P external input fluxes, and the fraction of gaseous losses of N to total (gaseous and leaching) losses of N from a global data set of ^{15}N measurements in soils
N Leaching (Tg N yr^{-1})	12	38	Wang et al., 2018	Data-driven estimates. See above
		28	Mayorga et al., 2010	based on a mass-balance approach for the land surface (watershed) and river system for year 2000
P uptake (Tg P yr^{-1})	43	26	Wang et al., 2018	Data-driven estimates. See above
P leaching (Tg P yr^{-1})	0.46	2.6	Wang et al., 2018	Data-driven estimates. See above
P occlusion (Tg P yr^{-1})	1.85	1.3	Wang et al., 2018	Data-driven estimates. See above

1381
1382
1383
1384
1385
1386
1387
1388
1389
1390
1391
1392
1393

1394
1395